Asymmetric forcing of convectively unstable transverse jets

Andrea Besnard ⬤, Elijah W. Harris ⬤, and Ann R. Karagozian ⬤*

Department of Mechanical and Aerospace Engineering, University of California,
Los Angeles, Los Angeles, California 90095, USA

The present paper explores the effect of asymmetric and helical excitation of the flow about the exit plane of a jet injected perpendicularly into crossflow. Both acetone planar laser-induced fluorescence and stereo particle image velocimetry were used to quantify transverse jet response at relatively high jet-to-crossflow momentum flux ratios ($J = 61$ and 41), which in the absence of external excitation produced a highly penetrating jet with a naturally convectively unstable upstream shear layer (USL) and asymmetric cross-sectional shape. For various excitation conditions, in some cases involving complete clockwise or clockwise perturbations and, in other cases, localized perturbations, alterations in the spectral character of the USL were observed, including lock-in to the applied frequency and quasiperiodicity involving applied and natural frequencies. For forcing frequencies and amplitudes producing lock-in, asymmetric excitation was found to accelerate USL vorticity roll-up and improved mean symmetry in the jet cross section. With these alterations in jet structure, molecular mixing between jet and crossflow fluid was improved in both center plane and cross-sectional planes of the transverse jet. Proper orthogonal decomposition analysis applied to the images revealed 2D and 3D mode coefficient plots with interesting topological features. In many cases, these phase diagrams revealed attractor like shapes, especially when excitation frequencies and amplitudes produced lock-in of the USL, suggesting that with further study, such topologies could be used as characteristic signatures for mixing optimization and low-order model development.

I. INTRODUCTION

The transverse jet or jet in crossflow (JICF) consists of a jet of fluid with mean velocity U_j injected perpendicularly or at an angle with respect to a crossflow of velocity U_∞. Typical flow interactions and vortical structures produced by flush injection of the transverse jet are shown in Fig. 1. In this figure, the jet coordinates are indicated (x, y, z) and the jet upstream shear layer (USL) trajectory is defined in terms of the parameter s. Nondimensional parameters commonly used to characterize the transverse jet include the jet-to-crossflow density ratio $S = \rho_j/\rho_\infty$, velocity ratio $R = U_j/U_\infty$, momentum flux ratio $J = \rho_j U_j^2/\rho_\infty U_\infty^2$, and the jet Reynolds number based on jet diameter D, $\mathrm{Re} = U_j D/\nu$. A Strouhal number $\mathrm{St}_o = f_o D/U_j$ may also be utilized, where f_o is the fundamental frequency of the jet's USL instability. Each of these parameters plays a role in the transverse jet trajectory, shear layer instabilities, jet spread, and dynamical characteristics, enabling the optimization of molecular mixing for specific flow conditions [1,2].

The transverse jet flow field is dominated by vortical structures identified in Fig. 1, most prevalent of which are the counter-rotating vortex pairs (CVPs) associated with the jet cross section [3,4], ringlike USL vortices [5], wrap-around horseshoe vortices [6], and upright wake vortices known
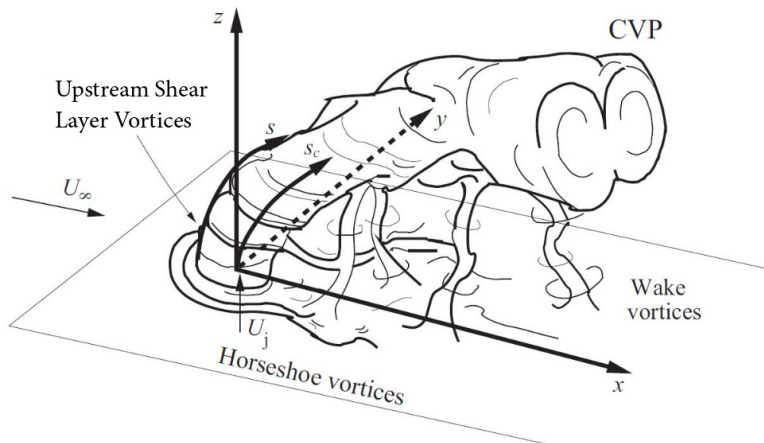
---

*ark@ucla.edu

FIG. 1. Schematic of the flush injected transverse jet and associated vortical flow structures. Orientation of coordinate axes x, y, z, jet upstream shear layer trajectory s, and jet centerline trajectory s_c are shown. Adapted from Ref. [7].

to draw wall boundary layer fluid into the jet [7]. The CVP dominates the jet cross section in the far field, and its evolution and structure are of interest to the current paper. The CVP is thought to promote entrainment of crossflow fluid into the jet, thereby enhancing mixing as compared with the free jet in quiescent surroundings [1,3,4,8], and primarily results from distortion of the vorticity in the jet shear layer. The nature of transverse jet shear layer instabilities and their response to external axisymmetric forcing are shown in recent studies to have a significant influence on JICF structure, dynamics, and molecular mixing characteristics [9–11]. Among the goals of the current paper is to extend this exploration to include the influence of asymmetric perturbations on the transverse jet.

A. Naturally occurring JICF instabilities and flow structures

The relevance of the transverse jet's USL to development of the CVP [3,4] has led to extensive experimental exploration of USL stability characteristics. Early studies involving hot wire anemometry to study USL spectral characteristics [5,12] reveal that as R or J are reduced, for a fixed jet Reynolds number, the USL transitions from being locally convectively unstable (CU), with a broadband fundamental frequency range and evidence of tonal interference between the shear layer and hot wire [13], to becoming globally or absolutely unstable (AU), with a strong pure-tone instability frequency and higher harmonics. For the equidensity JICF ($S = 1$), this transition from CU to AU occurs for jet-to-crossflow momentum flux ratios in the range of $J \approx 8 - 10$, depending on the jet and crossflow absolute viscosities and constituent gases [14]. For the low density JICF, the USL tends to be AU whenever $S \lesssim 0.45$, even for larger J values [15].

Direct numerical simulation (DNS) of the equidensity transverse jet flow field performed by Iyer and Mahesh [16] replicates the flush nozzle flow conditions explored in the experiments of Megerian *et al.* [5], for two different jet-to-crossflow velocity ratios, $R = 4$ and $R = 2$, straddling the experimentally observed transition condition near $R \approx 3.1$. Remarkably, the simulations for $R = 4$ produced a CU USL, while $R = 2$ produced an AU USL, with both qualitative and quantitative correspondence to experimental spectral characteristics. Later, global linear stability analysis (LSA) of the DNS [17] for these same flow conditions shows that for an AU USL at $R = 2$, the dominant eigenmode for the instability lies along the USL of the jet, while for the $R = 4$ case with a CU USL, downstream shear layer instabilities dominate. The simulations further indicate that a naturally AU transverse jet has a wave-maker region in the upstream near-field region of the jet, whereas the wave-maker region for a naturally CU JICF extends along the entire USL of the jet and wraps

around to the downstream side of the jet. These wave-maker regions identify locations for which the JICF could be more responsive to excitation, and in fact are consistent with recent experimental findings on the influence of the placement of small passive tabs at the interior periphery of the transverse jet exit plane [18].

More recent experimental studies have shown a clear relationship between the state of the transverse jet's USL [convectively versus absolutely (globally) unstable] and the jet's structure, especially in the jet cross section. Experiments in Getsinger *et al.* [19] employ acetone planar laser-induced fluorescence (PLIF) imaging to visualize jet structure, showing that a CU USL at large R or J values leads to a weakening of the shear layer vorticity roll-up, and consequently a susceptibility to the influence of asymmetric disturbances, often leading to the formation of an asymmetric CVP in the cross section. The asymmetric structure contrasts the relatively symmetric, clear CVP structure dominating the jet cross section at lower momentum flux ratios corresponding to an AU USL. This correspondence between the state of the USL instabilities and jet structure persists for a fairly wide range of jet Reynolds numbers. More extensive exploration of the influence of stability and jet structure on molecular mixing by Gevorkyan *et al.* [2] shows a significant correspondence between a symmetric jet cross section (typically for low J values) and enhanced molecular mixing. In contrast, a lesser degree of mixing between the jet and crossflow often takes place for the strongly asymmetric cross-sectional jet structure associated with a larger J and CU USL. Higher local USL strain rates and scalar dissipation rates are also associated with lower J values and AU flow, as quantified via simultaneous acetone PLIF and stereo particle image velocimetry (PIV) experiments [20]. Such trends also relate to augmented molecular mixing and transport processes, suggesting an ability to control such processes via altered flow conditions.

B. Axisymmetric jet excitation and response

In general, AU flows are known to be more difficult to control with applied excitation, while CU flows can be altered more readily with low-level axisymmetric excitation [21,22]. These features are borne out in experiments on axisymmetric excitation of the nonreactive transverse jet, including earlier studies incorporating smoke visualization [23] and more recent studies visualizing axisymmetrically excited jet behavior via acetone PLIF [10,11,24]. In addition to showing center-plane- and cross-section-based transverse jet structure in detail, acetone PLIF enables quantification of the effects of axisymmetric excitation on jet penetration, spread, and molecular mixing characteristics.

Axisymmetric temporal square wave excitation of the transverse jet demonstrates a significant influence on the case for a naturally AU USL in particular. Here, specific nondimensional stroke ratios, representing a nondimensionalization of the short temporal pulse during which jet fluid is introduced into the crossflow, can produce deeply penetrating, periodic vortices with improved jet penetration and spread. Enhanced jet penetration does not always correlate with improved molecular mixing, the latter being quantified via the unmixedness parameter [25–27], especially in the case of the naturally CU USL. There is a stronger correlation of improved mixing at higher J values with creation of a symmetric jet cross section via square wave excitation [10]. Double-pulse square wave excitation, producing the ability to control vortex ring interactions and collisions [24], show that for natural CU conditions, forcing which promotes vortex collisions provides the greatest enhancement in molecular mixing, whereas the jet with the AU USL produces the greatest enhancement in mixing when the vortex rings do not interact. Axisymmetric sinusoidal jet excitation itself [11] similarly demonstrates improvements in jet penetration, spread, and molecular mixing with strategically applied excitation, depending on the natural state of the USL. While the JICF with a CU USL typically has a naturally asymmetric jet cross section, appropriate sinusoidal excitation causes the structure to become more symmetric and the jet fluid concentration more evenly distributed between vortex pair lobes. Such results reinforce the traditional view that a symmetric CVP cross-sectional structure for the transverse jet leads to improved mixing over the free jet [1,28].

Yet the optimization and dynamical features of transverse jets exposed to axisymmetric sinusoidal excitation are more subtle than originally conjectured, and lock-in (LI) studies for the

equidensity transverse jet [9] provide special insights into USL response to such excitation. As is typical for naturally AU shear layers, including the low density or reactive free jet [21,29], when the transverse jet's USL is AU in the absence of forcing, applied sinusoidal forcing at a frequency f_f which is close to the fundamental frequency f_o can create a LI of the USL to f_f, where the dominant spectral peak appears at f_f and the natural instability associated with f_o virtually disappears and is thus suppressed. Excitation at forcing frequencies well above or below f_o requires higher amplitude forcing, resulting in a typical LI diagram defining the boundaries in frequency and amplitude to achieve this condition. Studies on the equidensity transverse jet [9] and the low-density free jet [21] demonstrate that the path to LI, as forcing amplitude is gradually increased, can include quasiperiodicity, in which two incommensurate frequencies appear (f_o and f_f), as well as linear combinations of the two.

For axisymmetric sinusoidal excitation of the transverse jet [9,11], there are additionally unusual and somewhat unexpected features, including clear (1:1) LI to the applied excitation frequency for both naturally CU as well as the expected AU USL conditions. There is a much higher forcing amplitude required to achieve LI when $f_f < f_o$ than when $f_f > f_o$, i.e., producing an asymmetric LI diagram for both CU and AU conditions. Moreover, the appearance of quasiperiodicity for both naturally CU and AU USL conditions is documented, as are improvements in molecular mixing under LI conditions, associated with either AU or CU USL conditions, the latter of which produces a more symmetric CVP in the jet cross section.

C. Helical instabilities and asymmetric jet excitation

Helical instability modes associated with transverse jets have only been studied to a limited degree, though such studies for the free jet have been much more extensive over the years, via LSA [30–36] as well as experiments [37–41]. The free jet is regarded to be axisymmetric close to the nozzle exit from the perspective of an open shear flow, where typically the spatial growth rate of axisymmetric mode ($m = 0$) is larger than for the first or second helical modes ($m = \pm 1$, $m = \pm 2$). If helical perturbations are present at the jet inlet, the axial symmetry of the mean jet profile can be disturbed [40], though if helical disturbance pairs $\pm m$ have the same amplitude as one another, the mean jet profile could still possess a plane of symmetry.

Azimuthal excitation of free jets in experiments can enable enhancement of helical modes and increased jet spread. For example, Cohen and Wygnanski [38] used eight azimuthally positioned speakers designed to blow air through narrow slits around the lip of a free jet nozzle; these studies, in addition to corresponding LSA, indicate that thinner mixing layers can amplify higher azimuthal modes ($m \geqslant 2$), while thicker layers only amplify axisymmetric ($m = 0$) and a single helical mode ($m = 1$). In other experiments, Kusek *et al.* [39] and Corke and Kusek [40] utilized an azimuthal array of 12 mini speakers placed close to the jet lip to excite helical mode pairs with the same frequency and equal but opposite azimuthal wave numbers, $m = \pm 1$, as well as axisymmetric modes, enabling the study of resonant growth of near-subharmonic modes affecting jet spread.

While the above-noted studies correspond to free jets ($J \to \infty$), local LSA by Alves *et al.* [42,43] shows that even a relatively small magnitude in crossflow velocity can affect stability characteristics. The nominally axisymmetric mode is found to be the most unstable mode in the transverse jet USL near-field region, upstream of the end of the potential core. LSA for both inviscid [42] and viscous [43] base flows representing the transverse jet shows increases in spatial growth rates and associated Strouhal numbers as the velocity ratio is reduced, consistent with corresponding experiments [5]. Local stability analysis of an inviscid transverse jet [42] further shows that the positive and negative helical modes $m = \pm 1$ can have different spatial growth rates at large R, suggesting the potential for an inherent weak asymmetry in the transverse jet. Susceptibility to such asymmetries at large R or J could explain in part the experimentally observed asymmetries in the CVP associated with the jet cross section [19].

Given the evidence that axisymmetric forcing can act to make the JICF cross section more symmetric, which in turn can improve molecular mixing, it is of interest to explore the effect of
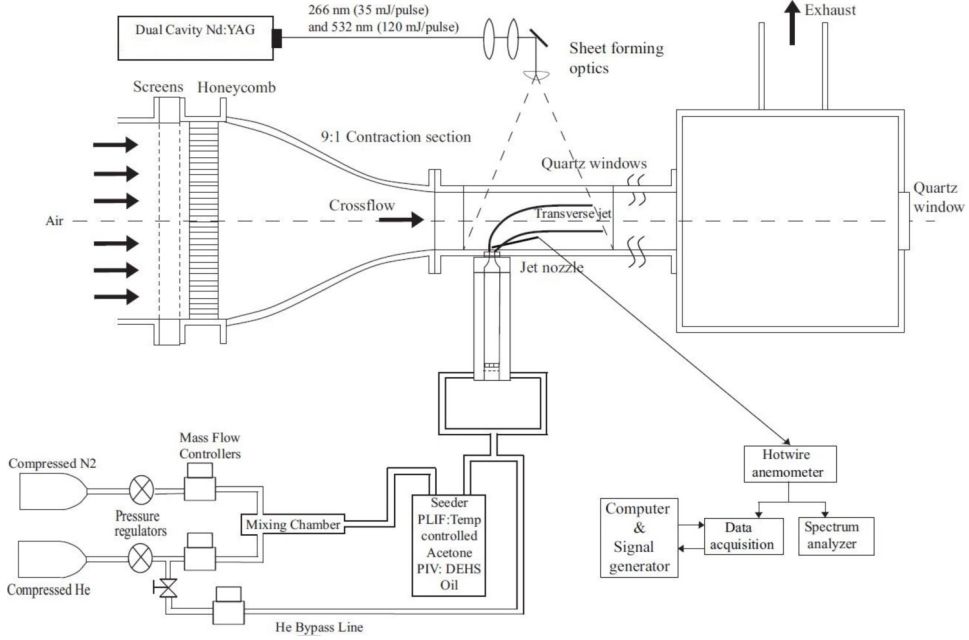
FIG. 2. Low velocity wind tunnel and associated experimental diagnostics for hot-wire anemometry, acetone PLIF, and stereo PIV.

asymmetric (external helical) forcing of the transverse jet on jet structure, mixing, and dynamical characteristics. It is of special interest to examine the effects of low-level asymmetric excitation on the JICF at larger momentum flux ratios (e.g., $J > 30$) where the cross section is naturally asymmetric for a flush nozzle-injected jet [19]. The present experimental study focuses on such asymmetric excitation, making use of the knowledge of stability characteristics of shear layers associated with both free and transverse jets, and taking advantage of the benefits of nonintrusive optical diagnostics in such explorations.

II. EXPERIMENTAL CONFIGURATION

A. Wind tunnel and experimental diagnostics

This experimental study was conducted in a low-speed wind tunnel whose general setup is shown in Fig. 2. A radial centrifugal fan, driven by a speed adjustable AC motor, used laboratory air to generate the crossflow. The crossflow stream passed through honeycomb flow straighteners and screens to condition the flow before entering a 9 : 1 area ratio contraction section. The crossflow then entered a test section where the flush nozzle-generated transverse jet issued perpendicularly. The test section floor had a removable portion which enabled different injection configurations within the overall wind tunnel framework. The specific floor used in this study, with asymmetric excitation near the jet exit, will be described in Sec. II B. The entire wind tunnel could be moved along the x-coordinate axis to fix the optical setup while interrogating different downstream cross-sectional y-z planes at different x locations using a linear stage controlled by a stepper motor. The jet fluid was fed through a symmetric four-way injection system into the jet plenum and passed through a long development section ($L/D = 155$) containing honeycomb flow straighteners to minimize swirl and ensure a spatially uniform jet. The conditioned flow was then fed into a nozzle ($D = 4.04$ mm) whose exit plane was flush with the test section floor. The flush nozzle used in the current study was designed with a

fifth-order polynomial contraction to generate thin jet shear layers at the exit, resulting in a free jet top-hat velocity profile in the absence of crossflow, as documented in prior studies [2,5].

In these experiments the gaseous jet mixture consisted of helium, nitrogen, acetone vapor, and Di-Ethyl-Hexyl-Sebacat (DEHS) oil, where the latter two species served as the tracers for acetone PLIF and PIV diagnostics, respectively. Bulk jet-flow properties were based on the mole fractions of the constituent species, room temperature, and room pressure, which are explained in detail in Ref. [44]. Flow rates for the He and N_2 were independently fixed by mass flow controllers (Tylan Model FC-260), and when performing simultaneous PLIF and PIV measurements, an additional controller (MKS GM50A) was utilized for a secondary supply of N_2 to allow for independent seeding of both tracer particles. For such experiments, the mixture of N_2 and He flowed into a temperature-controlled acetone seeder maintained in the vapor phase. Adjusting the mole fractions of various species enabled the desired density and jet Reynolds number to be achieved, as described in detail in Refs. [2,20]. The present paper is focused on equidensity ($S = 1$) jet conditions with $J = 61$ at Reynolds number Re = 2300, and with $J = 41$ at Re = 1900, both of which are shown to have CU USLs in the absence of excitation.

As in prior JICF studies, evaluation of the USL's spectral characteristics and evolution was made with a single-component constant temperature hot-wire anemometry probe (Dantec 55P15). The probe traversed along the USL and measured vertical velocity fluctuations, the signals for which were sent to a 90C10 constant temperature anemometry module and then after signal conditioning was fed into a dynamic signal analyser (HP-35665A), where power spectra were extracted over a span of 6.4 kHz at an 8 Hz resolution.

Nonintrusive acetone PLIF imaging was used in the present study to provide structure visualization as well as quantitative concentration measurements [45] enabling mixing characterization. For many of the acetone PLIF experiments, stereo PIV was performed simultaneously, enabling quantification of velocity and vorticity fields in addition to the scalar concentration field and associated metrics relevant to mixing. A dual-cavity Q-switched Nd:YAG laser (Quantel Evergreen 30266) operating at wavelengths of 532 nm (visible green, for PIV) and 266 nm (ultraviolet, for acetone PLIF) was utilized with independently tunable laser cavities so as to match the energy output between snapshots. Each cavity produced laser pulses at 8 ns full width at half maximum with UV and green energy levels of approximately 30 mJ and 200 mJ, respectively. The dual pulsed laser was operated at a repetition rate of 5 Hz so as to maximize the signal-to-noise ratio (SNR) of the UV to green light. The repetition rate, time increment between the cavities, and timing of the laser relative to the cameras were all controlled by a programmable external timing unit and LaVision's DaVis 8.2 software. All recorded data sets consisted of 500 instantaneous realizations of the flow field, more than sufficient to provide statistical convergence [46].

In the PLIF-only experiments, images were acquired using a 14-bit charge-coupled device (CCD) camera (LaVision Imager proX), fitted with a UV bandpass filter to pass only the acetone fluorescence wavelength of light. An external intensifier was used to amplify the fluorescence intensity and increase the SNR. The captured PLIF data images required postprocessing corrections to obtain accurate scalar concentration values, with details described in Refs. [44,46,47]. Following absorption correction, all images were normalized using the concentration of the jet potential core, which contained only jet fluid. Further details on calibration (including the self-calibration technique) and processing can be found in Refs. [2,44,47]. For these experiments, the imaging field of view (FOV) and final processed resolution provided pixel sizes in the range of 60–100 μm for both centerplane and cross-sectional views of the transverse jet. The resulting laser sheet thickness was quantified using the knife-edge technique, and found to be approximately 1 mm over the entire FOV. Prior work [20] shows that, for this diffusion-dominated flow field, the spatial resolution of the PLIF images was sufficiently resolved to quantify mixing metrics, being well below the conservative estimate of the strain-limited diffusion scale ($\lambda_d \approx 350 \,\mu$m), per Su and Mungal [48].

For the simultaneous PLIF and stereo PIV imaging, both UV and green light were utilized. The collimated laser beam was passed through a focusing optic before being turned and spread into a sheet by a UV-coated $f = -10$ mm cylindrical lens. The resulting laser sheet thickness was slightly thicker than for the high-resolution PLIF imaging, at approximately 1.4 mm over the entire FOV, so as to mitigate the loss of particles for PIV to out-of-plane motion. The PLIF images were recorded with a 12-bit internally intensified CCD camera (LaVision NanoStar) with image resolution of 1280×1040 pixels in contrast to the high-resolution PLIF-only experiments, which had an image resolution of 1600×1200 pixels. Hence it was determined that the higher-resolution PLIF images had an in-plane resolution of 34 μm per pixel, whereas the lower-resolution, PLIF portion of the simultaneous PLIF/PIV measurements, had an in-plane resolution of 65 μm per pixe1.

For PIV measurements, DEHS oil ($C_{26}H_{50}O_4$, LaVision 1108951) was seeded to the jet flow, and to visualize and quantify the velocity field of the crossflow, glycol-based smoke particles (0.2 μm mass-median diameter) were introduced by a commercial grade fog machine (Pea Soup Rocket) just outside the centrifugal blower. Stereoscopic PIV images were collected by two 14-bit cross-correlated CCD cameras (LaVision Imager ProX) placed on either side of the NanoStar camera that was utilized for the PLIF imaging. The two cameras were oriented through the side optical window of the tunnel, at angles displaced from perpendicular to the zx plane of approximately 22.5$^{\rm o}$, with the resulting offset yielding a 45$^{\rm o}$ separation between the two cameras. Further details on the PLIF/PIV diagnostics may be found in earlier papers [18,20].

B. Asymmetric excitation system

Based on prior findings that the JICF can improve molecular mixing when its cross section resembles a symmetric CVP [2], including jets at large momentum flux ratios J exposed to specific axisymmetric forcing conditions to create such symmetry [10,11], it is of interest to examine how asymmetric temporal excitation can achieve a similar influence on the jet. Further, given the benefits that a localized passive disturbance such as a tab can introduce for jet dynamics and mixing [18], consistent with JICF wave-maker regions identified computationally [17], it is especially of interest to explore localized temporal excitation that can impart different kinds of perturbations to the transverse jet. The conditions under exploration here included gaseous transverse jets at high momentum flux ratios, for cases with $J = 61$ (Re = 2300) and $J = 41$ (Re = 1900). The experiments with $J = 61$ corresponded to the higher resolution, PLIF-only cases, with mole fractions of 0.218, 0.234, and 0.548 for the acetone, He and N2, respectively. For the simultaneous PLIF-PIV tests at $J = 41$, the mole fractions of acetone, He, and N_2 were set at 0.112, 0.100, and 0.788, respectively, to account for the additional DEHS oil seeding while still maintaining a density ratio of $S = 1$. Per the analysis in Canzonieri [49], the maximum experimental uncertainty in jet density was 1.5% in the absence of acetone. With acetone present, the additional sources of error associated with the pressure and temperature control for the acetone seeder produced a maximum uncertainty of 5.1% in jet density [46].

In these experiments, asymmetric excitation was applied via four minispeakers (Tymphany PMT-30N18AL03-04) recessed into the test section floor, surrounding the flush-injected jet exit. The four speakers were spaced circumferentially at 90° with respect to one another, with centers located 3.625 cm from the jet center, as shown in Fig. 3. To distinguish individual speakers, they were numbered using the test section floor's x-y plane coordinate system, where the jet exit center served as the origin. The speakers were recessed within the test section floor and covered by a 0.05-mm-thick (0.002 inch) thin Teflon membrane so as not to disturb the JICF flowfield and crossflow boundary layer. It was verified that the incoming crossflow (wall) boundary layer profile encountered by the jet was not influenced by the presence of the flush speakers [50]; in the streamwise direction, the profile was consistent with the laminar flat plate Blasius boundary layer.

Each speaker could be individually operated with independent frequency, amplitude, and phase inputs, hence a wide range of forcing schemes could be employed. Each speaker was operated with calibrated frequency and amplitude signals via a specially designed control circuit. When all four
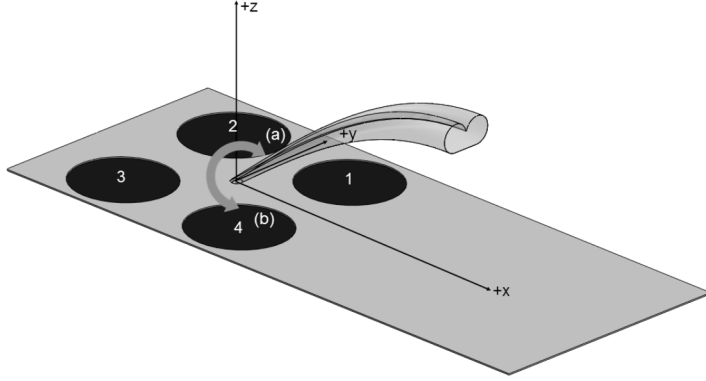
FIG. 3. Speaker configuration and numbering convention associated with external asymmetric forcing, where crossflow acts in the positive x direction. Operation of speakers in the sequence 2-1-4-3 created clockwise excitation (a), and 2-3-4-1 created counterclockwise jet excitation (b).

speakers were used, each one could be operated $90°$ out of phase with those adjacent to it (or at any other specified phase difference). This allowed controlled, relatively uniform, helical-like excitation of the crossflow fluid surrounding the jet in both clockwise (CW) (speaker sequence 2-1-4-3) and counterclockwise (CCW) (2-3-4-1) directions about the jet as shown in Fig. 3 as the temporal peak of the applied sine wave traveled about the jet. The orientation convention was the same as that of the jet cross section when viewed from the downstream end of the wind tunnel. The control circuit enabled the amplitudes of the pressure perturbations by each speaker to be matched, as measured by a microphone placed at the center of the jet exit. Speakers could also be operated individually, e.g., only speakers 2 or 3 or both, to study localized external perturbation effects. A comprehensive list of all speaker sequences used in this study [50] is summarized in Table I.

For these experiments, the $J = 61$ equidensity jet was excited with precisely controlled sinusoidal waveforms for each speaker with matched amplitudes and at frequencies above and below the fundamental frequency range obtained from USL spectral measurements, $f_o \cong 1600\text{-}1900$ Hz (shown in Sec. III A below). For the experiments at $J = 41$, the fundamental frequency was in the range $f_o \cong 1350\text{–}1600$ Hz, and there was similarly a range of excitation frequencies explored to enable determination of USL response, as will be described in Sec. III A.

TABLE I. Speaker operation sequences used to create directional or localized external perturbations.

Forcing scheme	Abbreviation	Speaker sequence
Clockwise, four speakers	CW 4	2-1-4-3
Counterclockwise, four speakers	CCW 4	2-3-4-1
Clockwise, upstream speakers	CW U	3-2-(1 off)-(4 off)
Counterclockwise, upstream speakers	CCW U	2-3-(4 off)-(1 off)
Clockwise, downstream speakers	CW D	1-4-(3 off)-(2 off))
Counterclockwise, upstream speakers	CCW D	4-1-(2 off)-(3 off)
Right side, upstream	RU	2
Left side, upstream	LU	3
Upstream speakers together	R and L	2 and 3 in phase
Right side, downstream	R D	1
Left side, downstream	L D	4

(a) $J = 61$ spectra

(b) $J = 61$ contour plot

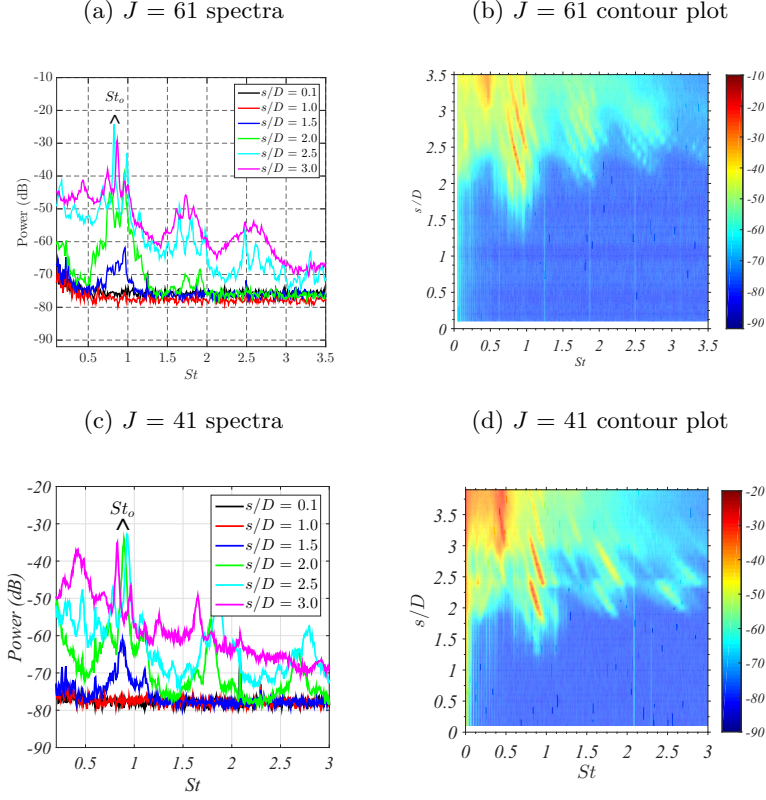(c) $J = 41$ spectra

(d) $J = 41$ contour plot

FIG. 4. Spectral characteristics of vertical velocity disturbances along the USL coordinate s/D for the unforced JICF, including discrete power spectra and spectral contour maps, respectively, for $J = 61$ [(a), (b)] and $J = 41$ [(c), (d)].

III. RESULTS

A. USL instabilities and response to excitation

As in prior studies, hot-wire anemometry enabled quantification of spectral characteristics along the USL, beginning at a location $s/D = 0.1$, and with spatial resolution increments of $s/D = 0.1$. Figure 4 shows spectral characteristics in the unforced USL for both $J = 61$ and $J = 41$, with instability frequencies f quantified in terms of the Strouhal number $St = \frac{fD}{U_j}$. Here Figs. 4(a) and 4(c) show spectra for distinct USL trajectory locations s/D, while data in Figs. 4(b) and 4(d) are more finely resolved spectral magnitude contour plots, in trajectory increments of $s/D = 0.1$, where the color bar corresponds to the disturbance magnitude. For both cases, the instabilities showed multiple peaks near a fundamental frequency f_o in addition to higher harmonics; in the better resolved contour plot, these multiple frequencies were manifested in frequency shifting of the dominant disturbance along the shear layer. This behavior is typical of the transverse jet's CU USL [5,15,23], though is not observed for the free jet. The frequency shifting is attributed to tonal interference by the hot wire with the strengthening shear layer [13]. For $J = 61$, spectral peaks occurred in the range $f_o = 1600$–1900 Hz, averaging $f_o \approx 1750$ Hz over the spatial range shown, while for $J = 41$, dominant peaks occurred in the range $f_o = 1350$–1600 Hz, averaging around $f_o \approx 1475$ Hz along the USL.

In the present paper, the influence of various kinds of asymmetric excitation on the response of the transverse jet's USL was investigated in detail. For most of the studies, the jet response was

measured via the hot wire placed fairly close to the jet exit, at the fixed USL trajectory location of $s/D = 2.0$ and positioned with the wire oriented along the x axis to effectively capture perturbations in the shear layer in response to external excitation. As noted above for axisymmetric excitation [9], such response can be characterized as involving a LI, quasiperiodic (QP) response, or no significant response (NSR). For asymmetric forcing, LI of the USL to sinusoidal forcing is considered to occur when the applied forcing frequency f_f causes the peak of the fundamental mode f_o at the s/D location in question to be diminished by three orders of magnitude or more, with the absence of any peaks at linear combinations of f_f and f_o, i.e., the absence of QP behavior. This criterion for LI is used in our earlier axisymmetric JICF excitation studies [9], and is similar to criteria used for LI studies involving the low density or reactive free jet [21].

Figure 5 provides a number of examples of USL velocity spectra at $s/D = 2.0$ for $J = 61$ experiments in response to operation of all four speakers in the CW or CCW manner, where the speakers act at matched frequencies and amplitudes (expressed in terms of the pressure perturbation P') with respect to one another. Note that the value of f_o at this particular USL location was closer to $f_o \approx 1725$ Hz. Figures 5(a) and 5(b) show the spectral responses to excitation of the four speakers at the same forcing frequency ($f_f = 1000$ Hz) but at differing amplitudes of speaker system operation. The first case, with forcing at a relatively low amplitude in Fig. 5(a), produced spectral peaks visible at the forcing frequency f_f but the fundamental at f_o was still clearly visible with excitation (red and blue lines). Peaks at linear combinations of f_f and f_o were also observed, and hence the condition in Fig. 5(a) was classified as being QP for either CW or CCW operations. With forcing at a somewhat higher amplitude, Fig. 5(b) shows that the fundamental peak at f_o was significantly diminished during excitation, and that only peaks at the forcing frequency and at its higher harmonics were observed to appear. For such conditions, the USL was considered to be locked in to the forcing.

Other cases in Fig. 5 provide examples of four-speaker excitation producing LI or near-LI conditions [Figs. 5(c) and 5(d)], QP conditions [Fig. 5(e)], and a condition within NSR to forcing [Fig. 5(f)]. It is particularly interesting to note that, at approximately the same amplitude of excitation for the cases in Figs. 5(b) and 5(e), gradually increasing the frequency of excitation demonstrated a transition from LI to QP, similar to what one would expect to produce in a typical LI diagram. At a relatively high frequency of excitation, $f_f = 3500$ Hz in Fig. 5(f), even at very high amplitude forcing (more than an order of magnitude above the other conditions in terms of pressure perturbation amplitude), one cannot achieve either LI or quasiperiodicity. This and numerous other excitation conditions documented in Besnard [50] suggested a consistency of the present asymmetric forcing with the notion of a LI diagram, as will be shown.

It is noted that the spectral responses of the USL in Fig. 5 were not precisely the same in terms of magnitude in response to CW as for CCW excitation. This observation could be related to natural asymmetries in the jet cross section typically observed at high momentum flux ratios [19], suggesting that the natural asymmetry could be related to unequal responses in the USL to external flow perturbations. An additional explanation may be related to the theoretical unequal helical growth rates ($m = \pm 1$) observed at large momentum flux ratios J in the LSA of Alves et $al.$ [42]. Forcing in one direction may enhance such natural asymmetries in the helical modes, while forcing in the opposite direction may work to suppress helical growth rates.

The dissimilarity in the response of the USL to directional application of four-speaker forcing led to an investigation of localized external forcing strategies. In some experiments, the two upstream speakers were operated in a semi-CW or semi-CCW way in which the upstream speakers were tuned to be 90° out of phase with each other, as in four-speaker operation schemes, but where the two downstream speakers were turned off, leading to directional forcing in the upstream portion of the flow field only. Other forcing strategies involved the opposite type of excitation, with only downstream speakers operating out of phase and upstream speakers turned off. Additional cases involved having the two upstream speakers forced together, in phase, to create more symmetric upstream excitation, as well as cases with purposeful asymmetric localized excitation, with only a single speaker operating.
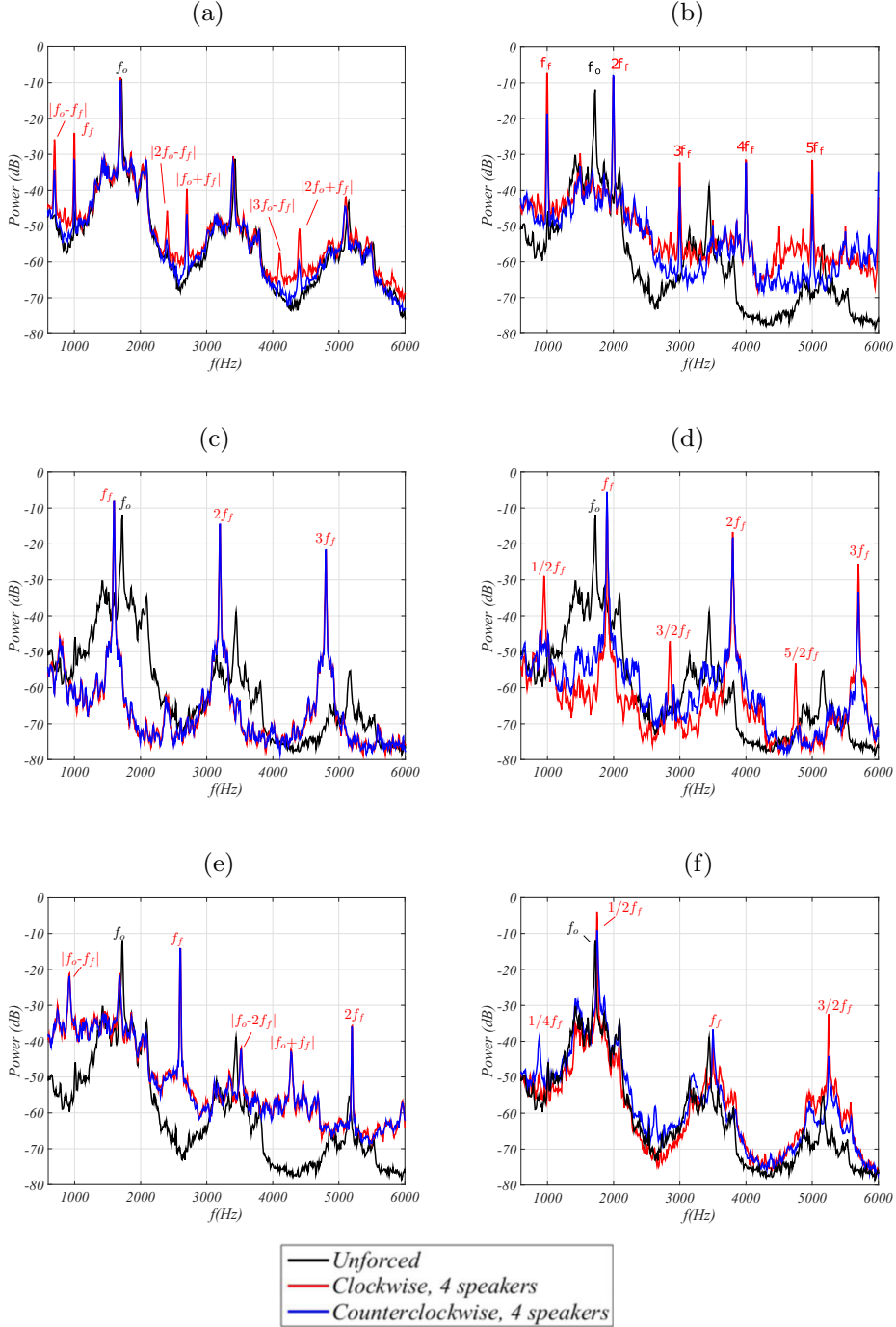
FIG. 5. Hot-wire-based vertical velocity spectra at $s/D = 2.0$ for the JICF at $J = 61$ and Re $= 2300$, with and without four speaker clockwise and counterclockwise asymmetric forcing, at various forcing frequencies f_f and pressure perturbation amplitudes. At $s/D = 2.0$, $f_o \cong 1725$ Hz. (a) $f_f = 1000$ Hz, P′ = 0.065 Pa, (b) $f_f = 1000$ Hz, P′ = 0.19 Pa, (c) $f_f = 1600$ Hz, P′ = 0.15 Pa, (d) $f_f = 1900$ Hz, P′ = 0.15 Pa, (e) $f_f = 2600$ Hz, P′ = 0.15 Pa, (f) $f_f = 3500$ Hz, and P′ = 2.0 Pa.
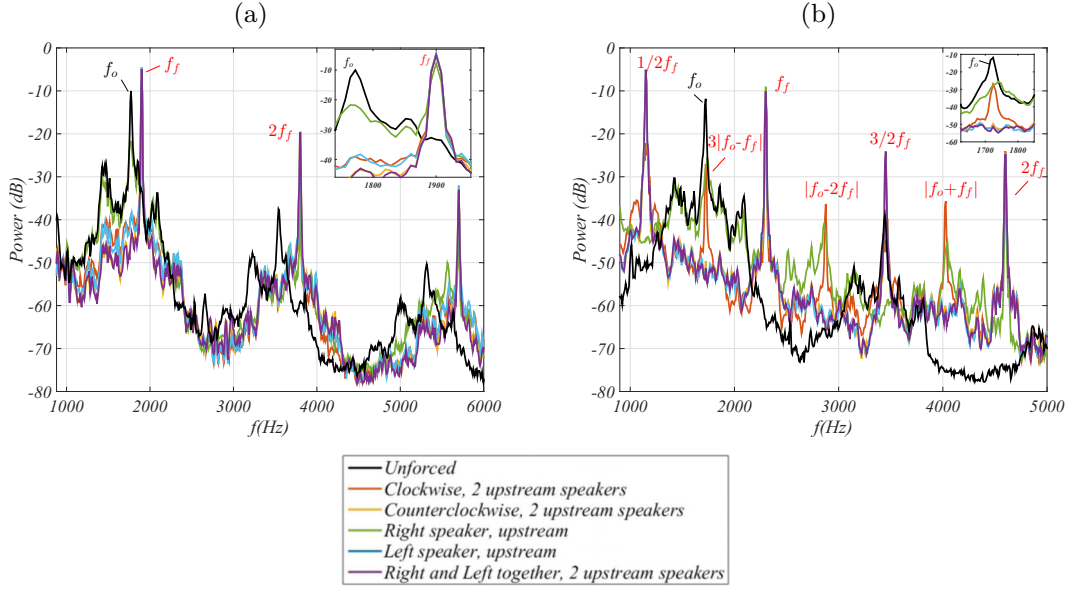
FIG. 6. Hot-wire-based vertical velocity spectra at $s/D = 2.0$ for the JICF at $J = 61$ and Re $= 2300$, with and without one- and two- speaker upstream forcing, at two different forcing frequencies f_f and pressure perturbation amplitudes. At $s/D = 2.0$, $f_o \cong 1725$ Hz. (a) $f_f = 1900$ Hz, P$' = 0.15$ Pa and (b) $f_f = 2300$ Hz, P$' = 0.28$ Pa.

Examples of USL velocity spectral responses for these alternative localized excitation approaches, for the $J = 61$ JICF, are shown in Fig. 6 for localized upstream speaker operation. As with four-speaker operation, the localized excitation for upstream (as well as downstream) excitation yielded some USL responses that exhibited LI, some with QP, and others with NSR. In Fig. 6(a), for example, LI was observed for all cases except for right upstream (RU) excitation, seen more clearly in the expanded inset, which was a bit surprising given the proximity of the forcing frequency ($f_f = 1900$ Hz) to the local fundamental frequency, $f_o = 1725$ Hz. In Fig. 6(b), with excitation at a higher frequency (2300 Hz) and an even higher amplitude of excitation (0.28 Pa), RU and CW operation of the upstream speakers (CW U) produced QP behavior, while all others demonstrated LI. The fact that localized left upstream (LU) and RU single speaker operation often resulted in differing power spectra traces suggested that USL response was perhaps not significantly related to unequal $m = \pm 1$ helical growth rates, since single-speaker operation would not necessarily induce a directional excitation azimuthally about the jet exit, but rather a localized perturbation; this will be discussed further below. For additional experiments involving downstream localized excitation [50], for the same excitation frequency and amplitude as in Fig. 6(a), all forcing conditions created LI, though there was similar nonsymmetric response observed between the right and left downstream excitation cases.

Local spectral results such as those shown in Figs. 5 and 6 can be used to produce maps of USL response conditions associated with various forcing strategies, similar to approaches commonly used to produce LI diagrams [9,21]. For the maps for various excitation conditions shown in Fig. 7, however (for the $J = 61$ case), there are responses corresponding to 1:1 LI as well as quasiperiodicity and NSR; these are indicated through the color coding. Figure 7 shows this mapping for the four-speaker study (a), upstream speaker study (b), downstream speaker study (c), and with superposition of all forcing conditions (d). The results in Fig. 7 show that, in general, when excitation was applied near the fundamental frequency f_o at a relatively low amplitude, the USL typically locked in to f_f, while applied excitation at a frequency well above f_o required a
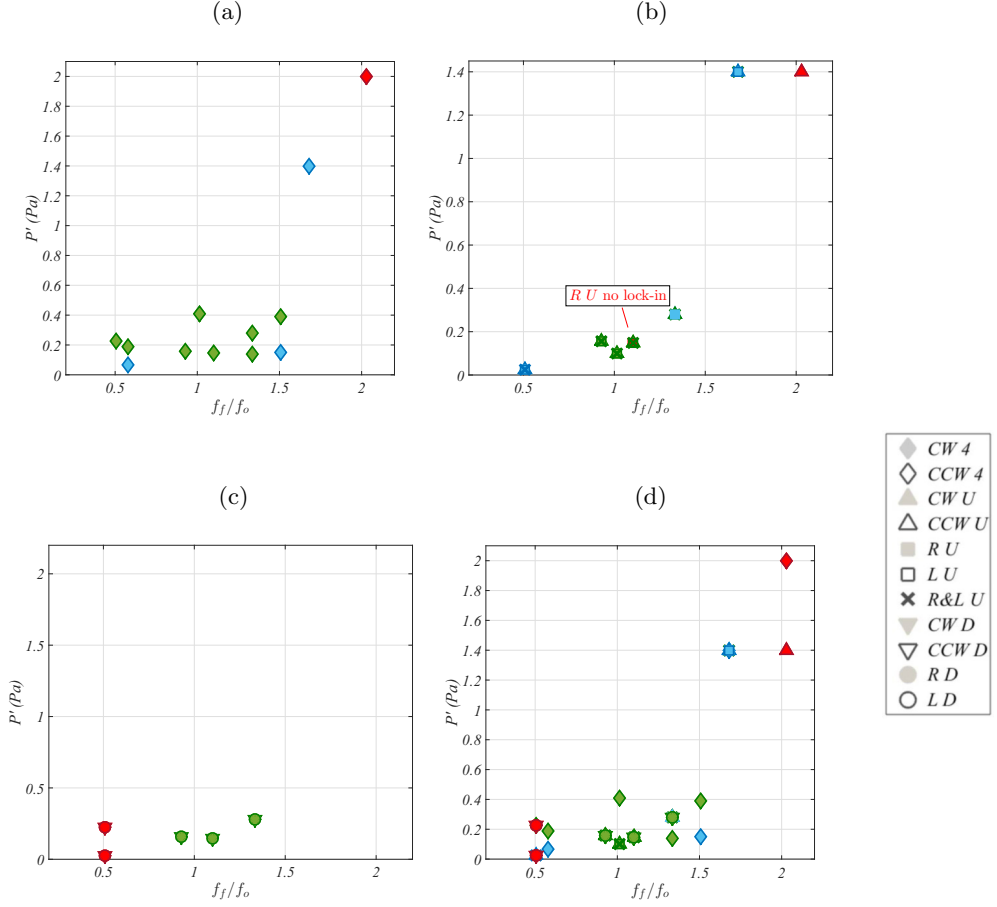
FIG. 7. Map of the USL response to external forcing at various forcing frequencies, modalities and perturbation amplitudes P', measured at shear layer location $s/D = 2.0$. Green colored symbols represent 1:1 lock-in of the USL, blue symbols represent quasiperiodic behavior of the USL power spectra, and red symbols represent no significant response of the USL to forcing (a) 4-speaker, (b) Upstream (2 and 1-speaker), (c) Downstream, (2 and 1-speaker), and (d) All conditions.

higher amplitude to even achieve quasiperiodicity, and when f_f approached $2f_o$, the USL did not show any significant response to excitation, at least for the highest amplitude possible with the current system. In contrast, at excitation frequencies somewhat below the fundamental, even as low as $f_f = 0.5f_o$, a relatively low amplitude of forcing still could create LI or quasiperiodicity. A somewhat anomalous case is indicated in Fig. 7(b) for low-level RU excitation at the upper range of the natural frequency ($f_f = 1900$ Hz, $P' = 0.15$ Pa), where the USL did not lock in to f_f, in contrast to other upstream excitation cases for this frequency and amplitude. It is possible that this unexpected finding resulted from a small asymmetry in the incoming wall boundary layer [19] or from natural unequal helical growth rates of the USL instability [42], though this requires further exploration. The overall asymmetry of the maps in Fig. 7(d) was similar to the nature of LI results in prior axisymmetric JICF excitation studies [9], including those for the naturally CU USL at a large J value, which is typically unexpected for such shear layers in general [51–53].
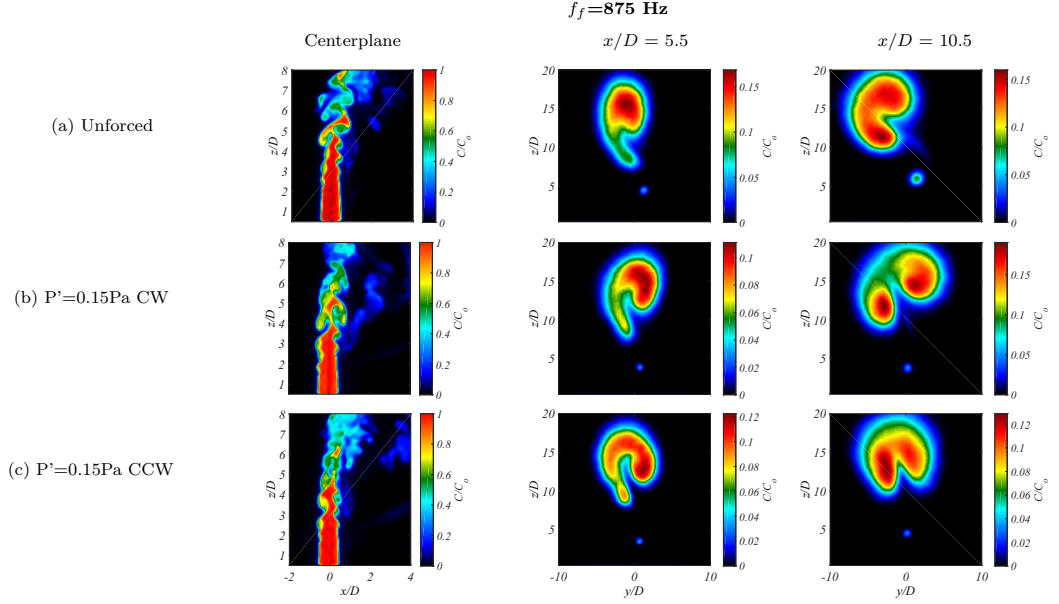
FIG. 8. Instantaneous center line and mean cross-sectional PLIF images in the y/D-z/D plane for the $J = 61$ JICF with $f_o \approx 1600 - 1900$ Hz. Shown are cases for unforced conditions (a) and 875 Hz excitation of all four speakers in the clockwise (b) and counterclockwise (c) directions, corresponding to QP and LI response of the USL, respectively.

B. JICF structural characteristics and mixing

Acetone PLIF imaging enables visualization of the effects of the various asymmetric excitation conditions, in addition to the ability to quantify these effects on jet-crossflow molecular mixing. In this section, we summarize these effects for the JICF case with $J = 61$ and Re $= 2300$, since this flow condition involved the high-resolution PLIF-only experiments, which provided greater accuracy in mixing quantification. Extensive acetone PLIF imaging was conducted for a range of asymmetric excitation cases, enabling visualization of the jet center plane in the x-z plane as well as cross-sectional slices at several downstream locations (in the y-z plane, in most cases at $x/D = 2.5$, 5.0, and 10.5 downstream of the jet center). Note that the cross-sectional scalar PLIF images were quantified using calibrated center-plane images (which included a known concentration in the potential core), using a thin seven-pixel-wide slice of the center-plane image at the same average x location of the jet, as described in detail in Ref. [2].

Figures 8 and 9 show PLIF images from a few of the many cases explored in Besnard [50]. In Fig. 8, even relatively low amplitude excitation of the four speakers close to the fundamental frequency range (1600 Hz) was observed to cause an earlier roll-up of the USL vortices as compared with the unforced condition (seen in the center-plane images). Both CW and CCW excitation conditions affected the CVP structure in the jet cross section. Interestingly, the case in Fig. 8(b) for CW excitation corresponded to an USL observed to be QP, per the response map in Fig. 7, while the CCW forcing case in Fig. 8(c) produced 1:1 LI. Such excitation produced different structural characteristics as well: the cross section for CCW excitation in Fig. 8(c) was somewhat more symmetric at $x/D = 5.5$ and 10.5 than for CW excitation effects shown in Fig. 8(b). The correspondence of improved symmetry with LI conditions was also observed for axisymmetric excitation of the CU JICF [11].

Sample results for jet structural alterations resulting from localized excitation are shown in Fig. 9, for both upstream excitation [Figs. 9(a)–9(c)] and downstream excitation [Figs. 9(d) and 9(e)], all
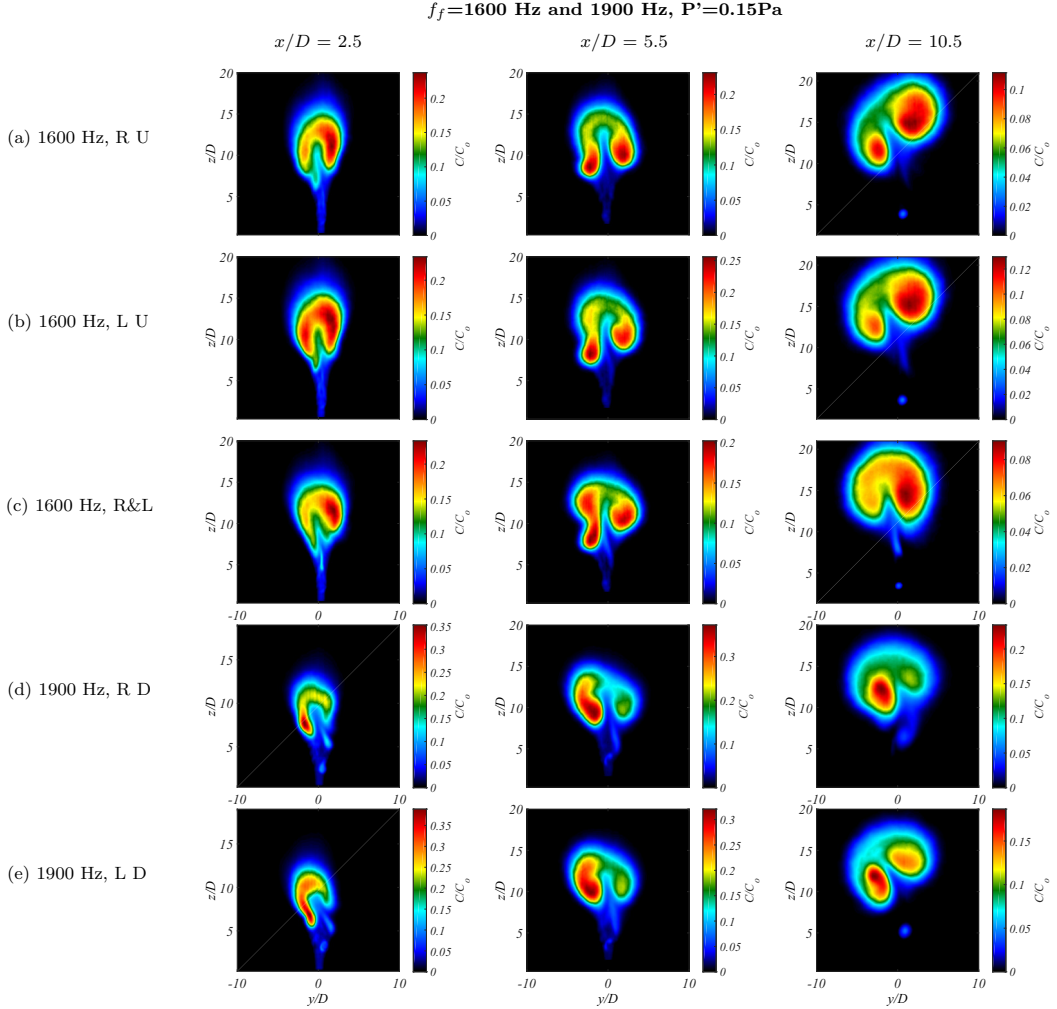
FIG. 9. Mean PLIF images in the cross-sectional y/D-z/D plane for the $J = 61$ JICF with localized excitation, each at amplitude $P' = 0.15$ Pa, and in all cases corresponding to lock-in [50]. (a)–(c) show $f_f = 1600$ Hz excitation in the upstream region and (d), (e) show $f_f = 1900$ Hz excitation in the downstream region.

at the same relatively low forcing amplitude of $P' = 0.15$ Pa, as examined in Fig. 8. Excitation frequencies here were at the bounds of the range of natural frequencies, $f_o \approx 1600$–1900 Hz, and in all cases in this set of figures, hot-wire measurements in the USL determined that LI conditions were produced. In all cases in Fig. 9, localized excitation produced cross sections that had more symmetrically oriented CVP-like cross sections than for the unforced case in Fig. 8(a), though to differing degrees. Interestingly, for upstream excitation, when both right and left speakers operated simultaneously at 1600 Hz, the cross section became more symmetric than for either right or left speaker operation. Downstream excitation also improved symmetry, as noted, though the fluid concentrated in the CVP lobes typically had a lesser degree of symmetry than observed for upstream excitation. Nevertheless, the fact that downstream excitation impacted jet structure to this extent suggested that flow perturbations in the JICF wake region could have a nontrivial effect on jet behavior. This observation on the influence of downstream excitation was in fact consistent with
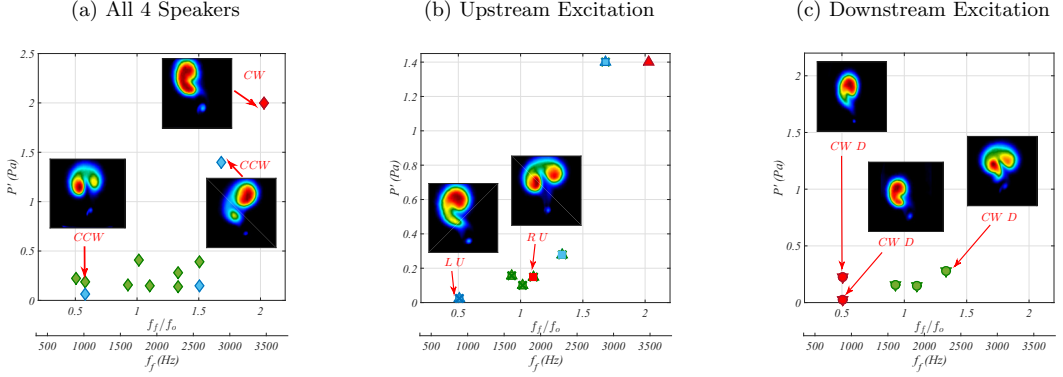
FIG. 10. Map of USL response, with representative mean cross-sectional jet PLIF images at $x/D = 10.5$, to various speaker operational configurations: (a) All four speakers, (b) local upstream forcing, and (c) local downstream forcing. Symbols correspond to the legend in Fig. 7, where conditions are identified as LI (green), QP (blue), and NSR (red).

JICF wave-maker regions identified computationally [17] for high momentum flux ratio transverse jets. As noted previously, these studies showed the wave-maker region to extend along the entire USL of the jet and wrap around to the downstream side, suggesting that perturbations in the downstream region could have an important influence at large J values.

These and many other high-resolution PLIF imaging results enabled us to explore the correspondence between USL response to asymmetric excitation (LI, QP, NSR) and altered JICF structure. Figure 10 revisits the maps of USL response to four-speaker, two-speaker, and one-speaker external forcing, with a few examples of jet mean cross-sectional structure associated with specific forcing conditions and responses. In Fig. 10(a) for four-speaker excitation, the condition for which there was NSR in the USL, $f_f = 3500$ Hz with a high amplitude pressure perturbation $P' = 2.0$ Pa for both CW and CCW operation did not result in any significant structural change, shown in the inset image. In contrast, with forcing at a much lower frequency ($f_f = 1000$ Hz, well below the fundamental range) and even a very low amplitude, $P'=0.19$ Pa, the locked-in USL was associated with a dramatically altered cross-sectional structure resembling a relatively symmetric CVP. For a USL response suggesting quasiperiodicity, e.g., with excitation at 2900 Hz and 1.4 Pa, the cross section was altered from the unforced shape but was not very significantly symmetric. For four-speaker excitation in general, all forcing conditions producing a locked-in USL in Fig. 10(a) produced a more symmetric cross section as compared to the unforced case, though the extent of symmetrization and overall shapes varied. Such effects align with the PLIF imaging results of axisymmetric sinusoidal forcing by Shoji *et al.* [11], in which the $J = 61$ cross-sectional structure was only clearly altered when the USL was locked in to the applied forcing.

The additional results shown in Fig. 10 for localized upstream forcing (b) and downstream two-speaker and one-speaker external forcing (c) show that the relation of USL LI to cross-sectional structure alteration was not as direct. For example, in Fig. 10(b), the previously mentioned unusual condition where low-level RU speaker operation did not result in LI and in fact produced NSR (now highlighted in red for emphasis at $f_f = 1900$ Hz and $P' = 0.15$ Pa), nevertheless resulted in dramatic structural changes and significant symmetrizing of the jet cross section as compared with unforced conditions. There were also cases in which QP USL response did not always produce structural changes in the cross section, e.g., in the LU forcing condition at $f_f = 875$ Hz and P'=0.025 Pa shown in Fig. 10(b). In Figure 10(c) with localized downstream excitation, there was a greater correspondence between LI and improved CVP/cross-sectional symmetry, and minimal structural changes corresponding to NSR in the USL.

High resolution acetone PLIF imaging in both the center-plane and cross-sectional views enabled quantification of jet-crossflow mixing characteristics for various excitation conditions for the $J = 61$ case. As noted in Gevorkyan *et al.* [2], transport processes at these low Reynolds number flows are primarily diffusion limited, hence molecular mixing is most relevant here. The unmixedness parameter U, which represents the second moment of the scalar field [25–27], was used in the present experiments, as in previous JICF studies, to quantify mixing. For example, in the y-z plane, the local unmixedness over the area $L_y L_z$ at an instant of time takes the form

$$U_{yz} = \frac{1}{L_y L_z} \iint \frac{(C/C_0 - \bar{C}/C_0)^2}{\bar{C}/C_0(1 - \bar{C}/C_0)} dy dz, \tag{1}$$

where C/C_0 is the local normalized value of scalar (acetone) concentration at a pixel element at (y, z), $\bar{C}$ is the spatial average over the domain, C_o is the calibrated concentration at the jet exit, and L_y and L_z are the length scales of the local jet interrogation area over which data are quantified. The local U can be evaluated in both cross-sectional (y-z) and center-plane (x-z) views. Comparison of unmixedness among different conditions was made possible by matching the mean concentration $\bar{C}$ at all locations in the flow field and for all flow conditions; this was achieved by altering the local interrogation area (i.e., $L_y L_z$) by adding or subtracting zero-valued pixels. The unmixedness calculation is applied to each scaled instantaneous image at each location and then averaged over the entire data set, typically consisting of 500 images [2,44]. Unmixedness is quantified on a scale of $0-100\%$, where a lower unmixedness corresponds to a more homogeneous, well-mixed flow field.

Quantification of unmixedness for a range of asymmetric excitation conditions was performed based on the high resolution PLIF imaging [50]; a few examples are shown in Figs. 11 and 12 for both center-plane- and cross-section-based unmixedness, $U_{c,xz}$ and U_{yz}, respectively. For the latter results, examples of mean cross-sectional shapes are shown, in addition to an identification (by a circle) of the more symmetric cross sections. Typically, there was a consistency between the better mixing cases (i.e., the lower U values and trends) for both $U_{c,xz}$ and U_{yz} parameters. For example, for four-speaker excitation at lower frequencies, shown in Figs. 11(a) and 11(b), the greatest improvements over the unforced mixing were achieved in both planes for cases with excitation close to the fundamental, at $f_f = 1600$ Hz under CCW conditions and 1000 Hz under CW conditions. Such cases tended to have more symmetric cross sections. At higher excitation frequencies for four-speaker operation in Figs. 11(c) and 11(d), one similarly finds some correspondence between cross-sectional symmetry and better molecular mixing. For the four-speaker operation, there was general correspondence between improved mixing and LI of the USL, though it was not always the case that most symmetric cross sections produced the best mixing. It also should be noted that all four-speaker CW and CCW forcing cases produced enhanced mixing to some degree, even when the USL was known to exhibit QP behavior or was not locked in to the asymmetric forcing. And with excitation at very high frequencies in comparison with the fundamental frequency range, mixing improvement was significantly diminished.

For more localized forcing, jet cross-sectional structure symmetry and superior mixing were more closely correlated, though, interestingly, USL LI and such symmetry were not as closely correlated, as discussed earlier. For example, for upstream localized excitation in Figs. 12(a) and 12(b), the strongly symmetric JICF produced by LU and RU speaker excitation (together) corresponded to the lowest unmixedness in both planes, with RU operation produced similar benefits.

In comparing full CW and CCW excitation of four speakers with two or one speaker operation, however, it is noted that four-speaker operation generally led to greater improvements in mixing (lowered unmixedness) than localized excitation. In fact, in comparing Figs. 11 for four-speaker actuation and 12 for local speaker operation, one observes that full CW or CCW excitation always improved mixing, while for some limited localized excitation cases, unmixedness actually increased, meaning a worsening of molecular mixing. For such localized excitation conditions, there was sometimes but not always a direct correspondence between worsening center-plane and
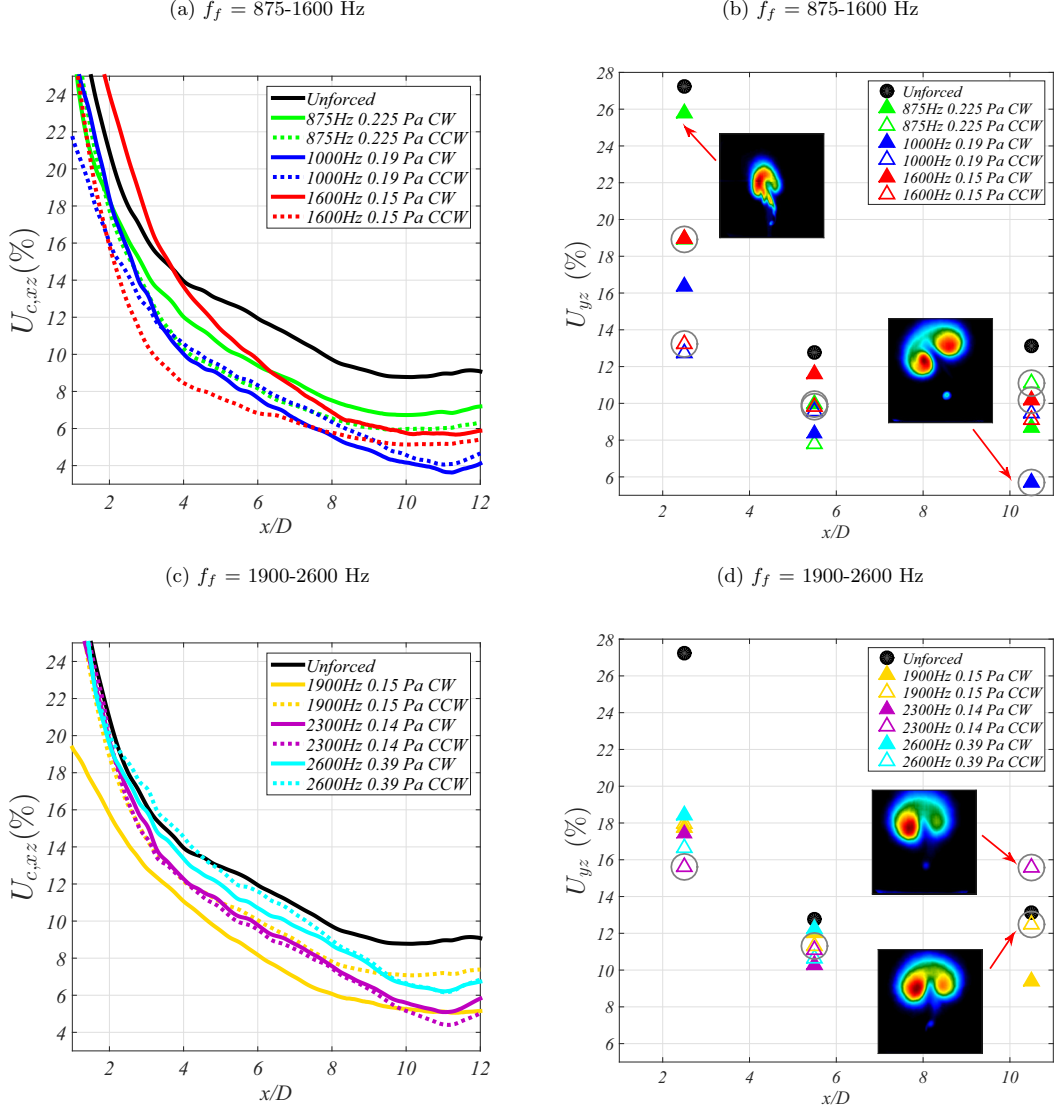
(a) f_f = 875-1600 Hz

(b) f_f = 875-1600 Hz

(c) f_f = 1900-2600 Hz

(d) f_f = 1900-2600 Hz

FIG. 11. Unmixedness in center plane ($U_{c,xz}$) and cross-sectional (U_{yz}) planes for $J = 61$ at various excitation conditions: (a) Four-speaker operation at frequencies at or below the fundamental range and (b) four-speaker operation at frequencies at or above the fundamental range. Circles represent forcing cases with the most symmetric cross section. Select mean jet cross-sectional PLIF images are inset.

cross-sectional mixing and a more asymmetric jet cross section. Yet when excitation took place much closer to the natural frequency range, improved symmetry and mixing were observed [50].

C. USL vorticity and scalar field correspondence

Simultaneous PLIF and PIV can provide additional insights into the effects of asymmetric excitation on transverse jet behavior, including related dynamical phenomena that can affect molecular mixing. These experiments were conducted for the case of the equidensity JICF at $J = 41$ and Re $= 1900$, which, according to the spectral characteristics in Figs. 4(c) and 4(d), also had a CU
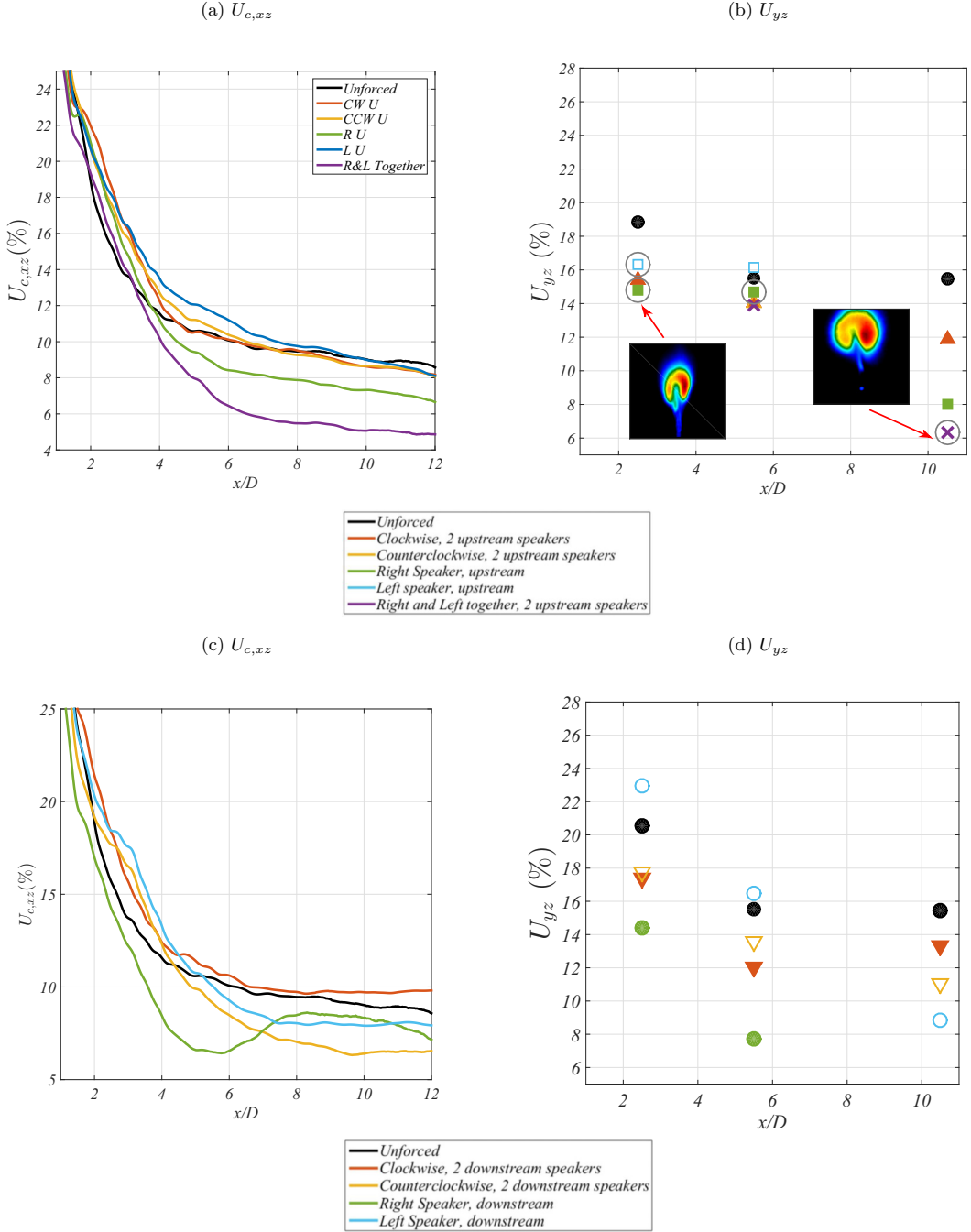
(a) $U_{c,xz}$

(b) U_{yz}

(c) $U_{c,xz}$

(d) U_{yz}

FIG. 12. Unmixedness in (a), (c) center plane ($U_{c,xz}$) and the (b), (d) cross-sectional (U_{yz}) planes for $J = 61$ at localized excitation conditions at $f_f = 1600$ Hz and P' = 0.15 Pa corresponding to upstream excitation (a), (b) and downstream excitation (c), (d). Circles represent forcing cases with the most symmetric cross section. Select mean jet cross sectional PLIF images are inset.
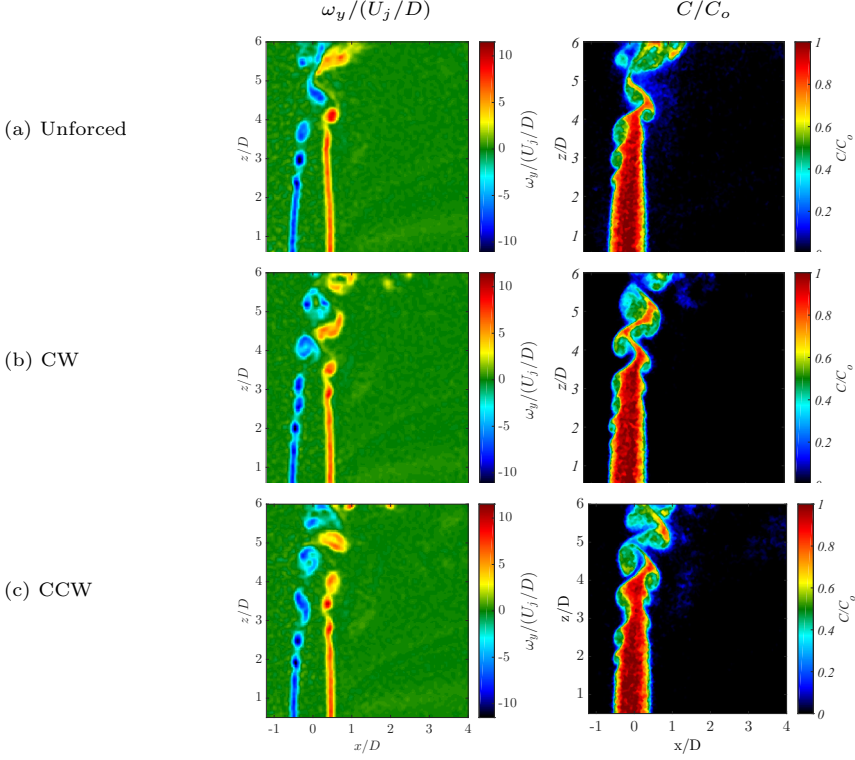
FIG. 13. Instantaneous simultaneous PLIF/PIV imaging of the $J = 41$ JICF. Data shown for scaled vorticity $\omega_y/(U_j/D)$ and scaled jet fluid concentration C/C_o in the center-plane view for the (a) unforced case and (b), (c) subject to directional forcing with excitation $f_f = 1600$ Hz and P'= 0.15 Pa.

USL in the absence of excitation. Figure 13 shows simultaneous instantaneous vorticity and scalar fields extracted from PIV and PLIF imaging, respectively, in the center plane of the JICF at $J = 41$, for unforced and forced conditions. Corresponding cross-sectional images at the center of the jet exit ($x/D = 0$) are shown in Fig. 14. Forced cases here corresponded to four-speaker asymmetric excitation at a frequency and amplitude for which there was documented USL LI to the applied excitation. As observed in prior experiments for the unforced JICF [20], the vorticity field and the scalar concentration field produced similar structural characteristics to one another, especially with respect to the shear layer vorticity rollup and evolution in both upstream and downstream regions. As noted above, the PLIF portion of the simultaneous PLIF (PIV) imaging was captured with a camera of lower resolution than that for PLIF-only experiments and without a signal intensifier. Small variations in the crossflow seeding density over the duration of the experiment affected instantaneous laser energy absorption, hence PLIF images in these figures tended to be noisier than those for high resolution PLIF-only experiments.

As indicated in PLIF-only centerplane images [e.g., in Figs. 8(b) and 8(c)], asymmetric excitation using four speakers produced more rapid USL vortex roll-up, for either CW or CCW operation, as compared with unforced results. This is now confirmed by both instantaneous vorticity as well as scalar fields in Figs. 13(b) and 13(c). Cross-sectional instantaneous images in Fig. 14 suggested that at the center of the jet exit ($x/D = 0$) for this high-momentum flux ratio case, the vorticity as well as scalar structure were generally symmetric, though very small cross-sectional alterations associated with helical excitation were observed, in addition to a slight shortening of a potential corelike region. These small asymmetries observable in the cross section at the exit were manifested in more
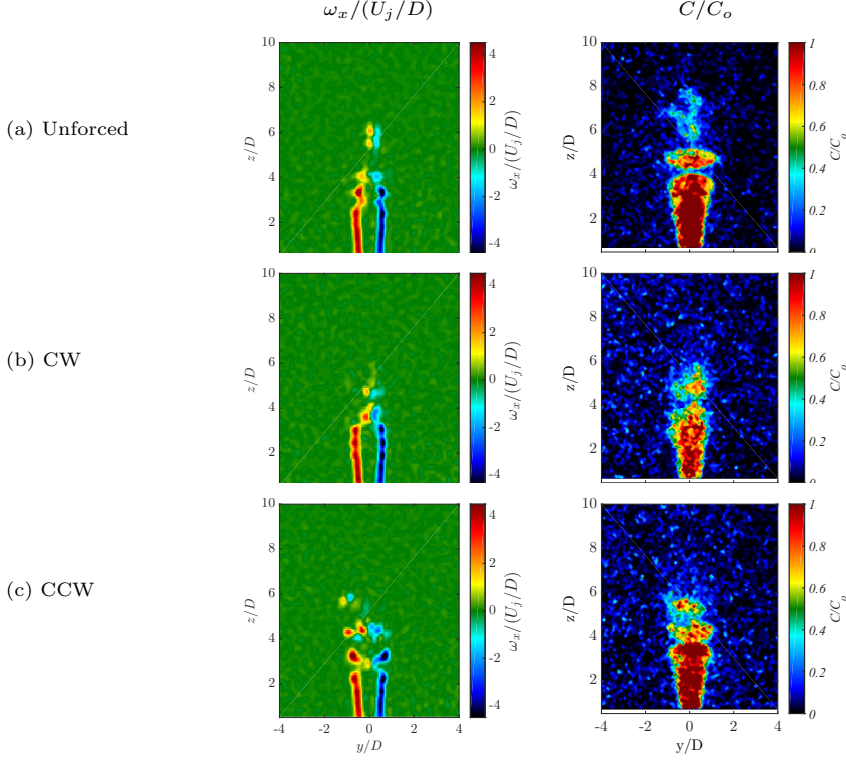
FIG. 14. Instantaneous simultaneous PLIF/PIV imaging of the $J = 41$ JICF. Data shown for scaled vorticity $\omega_x/(U_j/D)$ and scaled jet fluid concentration C/C_o for the $x/D = 0$ cross-sectional view (a) unforced case, and (b), (c) jet subject to clockwise and counterclockwise directional forcing with excitation $f_f = 1600$ Hz and P'= 0.15 Pa.

significant cross-sectional asymmetries developing further downstream as shown in Fig. 8. Similar features to those in Figs. 13 and 14 were observed in center-plane and cross-sectional imaging for excitation cases with localized operation (e.g., CW U, RU, LD, and so forth). At or very close to the jet exit, however, asymmetry was not a significant feature, even in the absence of excitation [50].

Simultaneous PLIF and PIV capture of the transverse jet flow field also enabled extraction of local average strain rates and scalar dissipation rates in the vicinity of the USL [50], incorporating methods described in detail in Gevorkyan *et al.* [20]. As expected (not shown), vortex roll-up in the USL corresponded to increases in both local average strain rate and scalar dissipation rate, quantified by PIV and PLIF imaging, respectively. Thus, the effect of asymmetric excitation on accelerating USL vorticity roll-up in the center plane, e.g., as indicated in Fig. 13, had the corresponding effect of moving the peak in the spatial evolution of strain rate or scalar dissipation rate further upstream. Additional details on these observations may be found in Besnard [50].

D. POD analysis and dynamic response to asymmetric excitation

The influence of asymmetric excitation on JICF dynamics, beyond alterations to spectral content in the USL described previously, may be explored via snapshot proper orthogonal decomposition (POD) [54]. Snapshot POD may be applied to the scalar concentration fields extracted from acetone PLIF as well as velocity vector fields extracted from stereo-PIV imaging. This approach has been explored in fundamental studies of the unforced JICF [20,55,56] as a means of extracting mode

structures from instantaneous snapshots of the flow; more recently it has been used to examine the effects of passive tabs on JICF dynamics [18].

Snapshot POD analysis was applied in the present experiments to all 500 instantaneous realizations of the flow field for each test case considered, for both high-resolution PLIF as well as the simultaneous PLIF/PIV experiments. 500 snapshots exceeded the 300 snapshots required for statistical convergence for this flow field; further details on this determination can be found in Shoji [46]. Proper orthogonal mode structures were ordered corresponding to their magnitudes of total kinetic energy fluctuation, helping to reveal characteristic flow features and dynamics for various cases, in particular those associated with the influence of asymmetric and local external excitation.

For example, Fig. 15 shows the first two velocity and scalar mode structures (modes 1 and 2) and their corresponding portions of fluctuating kinetic energy (KE, extracted from PIV) and scalar energy (SE, extracted from PLIF) content for the unforced JICF at $J = 41$. As noted previously, for this case the USL fundamental frequency was in the range $f_o \cong 1350$–1600 Hz. As expected, in the center-plane view [Figs. 15(a) and 15(b)], the first two PIV and PLIF POD mode structures and proportional energy contributions aligned well with the results reported by Gevorkyan *et al.* [20] for the flush nozzle-generated equidensity $J = 41$ JICF. The PIV and PLIF POD modes in the cross-sectional plane at the jet orifice upstream edge ($x/D = -0.4$), shown in Figs. 15(c) and 15(d), suggest that the first PIV mode (c1) captured the crossflow and its deflection around the jet, as indicated by the in-plane velocity arrows outside of the jet core. Interestingly, the pattern of crossflow motion showed a definite CW directional preference above $z/D \approx 3$, corresponding to the location of USL roll-up initiation and suggesting possible initiation of the asymmetry in the USL. This distinct directionality was only marginally observed in the second PIV POD mode, which appeared to capture periodic shear layer roll-up. The first two modes at the cross-sectional plane at the center of jet injection, $x/D = 0$ [Figs. 15(e)–15(f)], captured more symmetric vorticity and scalar dynamics, consistent with Fig. 13(a).

Correspondence between PIV-based POD mode structures and simultaneously captured PLIF-based POD mode structures for jets exposed to asymmetric excitation paralleled those shown in Fig. 15, especially in the centerplane [50]. Because of the improved image quality in high-resolution PLIF-only images and associated snapshot POD modal structures, results for these higher resolution experiments will be emphasized in the subsequent discussion here, for the JICF at $J = 61$ and with a fundamental USL frequency range of $f_o \cong 1600$–1900 Hz. For example, Fig. 16 shows PLIF-based POD mode structures for unforced as well as asymmetric forcing conditions at this higher J condition. Once again, these POD mode plots indicated that asymmetric forcing of four speakers produced much earlier shear layer rollup in both upstream and downstream layers, as well as an increase in scalar energy content for the proper orthogonal modes as compared with the unforced case. The excitation cases here produced USL LI, per Fig. 7. Interestingly, here CCW forcing of all four speakers resulted in pairing of the first two modes, as seen in fluctuation scalar energy content and appearance; this was not the case for CW excitation, which produced more sinuouslike structures. Such differences suggested that dynamical characteristics of the asymmetrically excited JICF could be dependent on the specific type of forcing, and these differences (examined in more detail below) may explain some of the differences observed in earlier mixing characteristics.

POD analysis enables one to analyze fluctuations in magnitude of the various mode coefficients across the series of original snapshots [20,55,57], and thus to study correlations in the evolution of the flow dynamics. If the mode coefficients from specific mode pairs are then plotted against one another, one can determine if the modes are correlated in their evolution over time. For the transverse jet, when the USL is AU at relatively low momentum flux ratios J (typically less than 10), it has been documented that plots of the first two proper orthogonal mode coefficients against one another resemble a ringlike structure suggestive of a periodic traveling wave [18,20]. This implies that the dominant jet dynamical behavior may be characterized by linear combinations of the first two modes. In contrast, these prior studies show that for the JICF at larger J values with a CU USL, the plot of the first two mode coefficients typically deteriorates into a diffuse blob, without clear single frequency-based periodicity, illustrating the broadband frequency content of shear layer
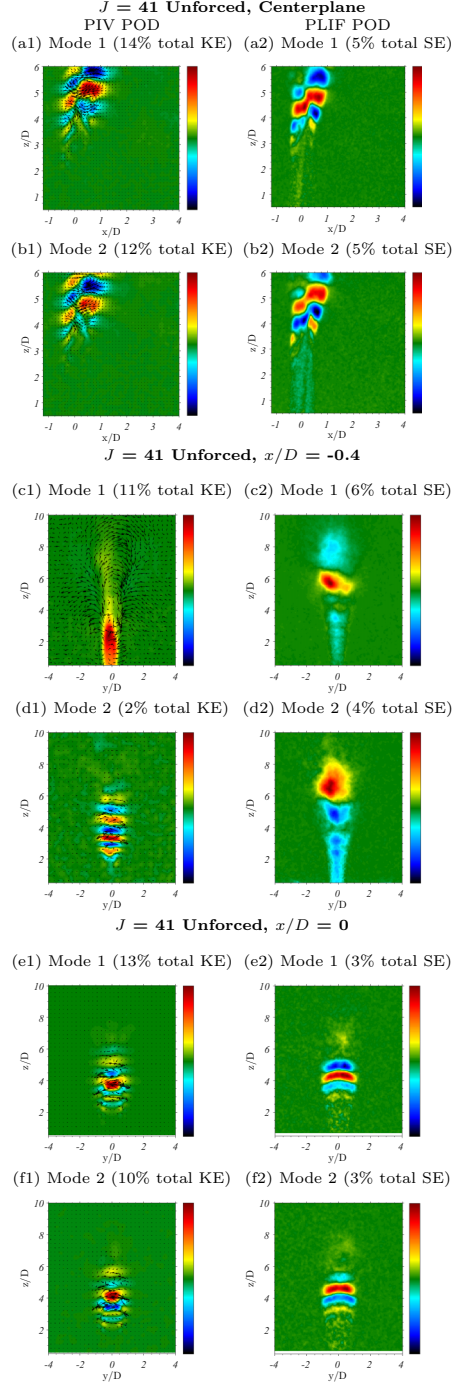
FIG. 15. PLIF and PIV POD mode structures extracted from instantaneous images of the unforced $J = 41$ JICF in (a), (b) center-plane view; (c), (d) upstream cross-sectional view at $x/D = -0.4$; (e), (f) jet center cross-sectional view at $x/D = 0$. Percentage of total kinetic energy (KE) or scalar fluctuation energy (SE) contributed by each mode is indicated. The color bar in each image represents the mode scaled by its own norm and the mean jet velocity at the jet exit U_j.

$J = 61$ Unforced, Centerplane

(a1) Mode 1 (4% total SE)   (a2) Mode 2 (3% total SE)

f_f = 1000 Hz, P'= 0.65 Pa CW4, Centerplane

(b1) Mode 1 (28% total SE)   (b2) Mode 2 (19% total SE)

f_f = 1000 Hz, P'= 0.65 Pa CCW4, Centerplane

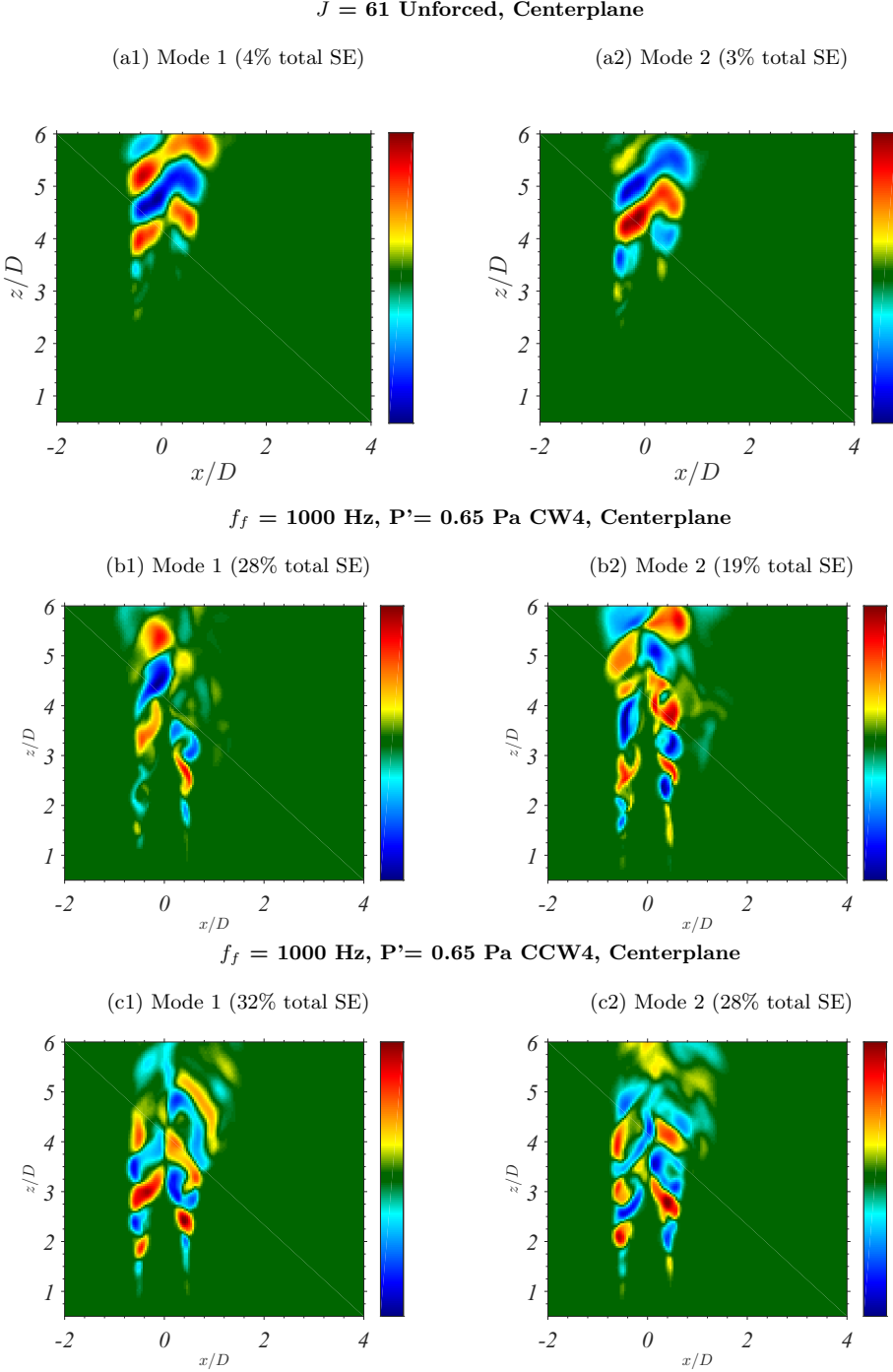(c1) Mode 1 (32% total SE)   (c2) Mode 2 (28% total SE)

FIG. 16. PLIF POD mode structures from instantaneous center-plane images of the $J = 61$ JICF for (a) unforced conditions and four-speaker forcing at $f_f = 1000$ Hz and P'$= 0.65$ Pa, under (b) clockwise and (c) counter-clockwise operation. Percentage of total scalar fluctuation energy (SE) by each mode is indicated. The color bar in each image represents the mode scaled by its own norm and the mean jet velocity at the jet exit U_j.

instabilities in a CU flow. This approach was used in the present study for both high-resolution PLIF-based and PLIF/PIV-based POD modal exploration. Snapshot POD coefficients of the first two modes pairs were investigated, in addition to the 3D phase space formed from the three most dominant POD mode coefficients [50]. Because POD analysis evaluates a system as a series of differential equations, phase portrait mapping of the mode coefficients represents the solution space to the equations, where the dominant modes represent the least unstable solutions. In this sense, phase portrait mapping of the POD mode coefficients is analogous to Poincaré's analysis of the solution curves defined by differential equations [58], where if there are several unstable solutions in the steady state, a time signal will oscillate around the least unstable solution(s).

Figures 17 and 18 plot the POD mode coefficients for sample cases of the four-speaker PLIF-only study, with comparison to the unforced $J = 61$ jet results. In these and subsequent plots, black symbols represent the POD mode coefficients associated with the unforced jet, green colored symbols represent conditions where separate hot-wire studies indicated 1:1 LI of the USL, blue symbols represent QP behavior of the USL power spectra, and red symbols represent conditions where NSR of the USL to external forcing was found via hot-wire spectral measurements. Yellow symbols indicate that the nature of the USL for the forcing condition had a character which was not directly measured via the hot wire, but often could be inferred from maps such as those indicated in Fig. 10 to be either locked-in to the forcing or demonstrating quasiperiodicity, as will be indicated below.

As expected, in the absence of external excitation, the phase portraits in Fig. 17(a) for $J = 61$ did not produce periodicity in the POD coefficients. The random-appearing blobs of points, each corresponding to mode coefficient values for each of the 500 realizations, were consistent with previously explored CU JICF conditions [20]. When CW or CCW forcing of the four speakers was applied below the fundamental frequency but with LI of the USL, e.g., at $f_f = 1000$ Hz at an amplitude of 0.65 Pa, as in Figs. 17(b) and 17(c), the 3D representation of the first three coefficients always produced a multiprongedlike structure which often twisted as it developed in the third dimension. We note that for this 1000 Hz four-speaker excitation, the similarities in modal shapes between CW and CCW operation, shown in Fig. 16, did not manifest in significant differences in the mode coefficient plots, shown for the same conditions in Figs. 17(b) and 17(c). We note that in general, tripled patterns often emerged in other forcing conditions from the first two modes, which perhaps suggested three different preferred combinations of paired dominant modes over the ensemble of 500 images. A few forcing cases associated with LI also produced patterns in the coefficients of the second mode pair, a_3 and a_4, as seen for 1000 Hz excitation, suggesting a secondary recurring relationship in the flow field. It is noted that other JICF studies, such as in the computational studies of forced jets by Bidan *et al.* [59], indicate 2D phase portraits in which the POD coefficients are similarly clustered into nodes or preferred locations, with the first pair of POD coefficients assuming a starlike shape under specific forcing conditions.

For excitation conditions very close to the fundamental range, e.g., at a frequency of 1750 Hz, much lower amplitude excitation was required to achieve LI, per Fig. 10(a), and as such, the phase portraits for this frequency, shown in Figs. 17(b) and 17(c), very likely corresponded to LI conditions. Unlike the case with 1000 Hz excitation, however, the differences in dynamical characteristics between CW and CCW forcing were more distinct, though both exhibited periodicity in the coupling among modes. Interestingly, CCW excitation close to the fundamental range in Fig. 17(e) produced a more complicated periodic oscillation pattern for the a_3 versus a_4 plot, resembling a torus or trefoil knot shape. In fact, the 3D phase portrait for this case also had an unusual shape, similar to that of a Rössler-like attractor, and this kind of dynamical behavior was seen in other asymmetric excitation conditions. For example, for four-speaker 2300 Hz excitation, determined to produce LI, shown in Fig. 18(a), CW excitation produced a trefoil knotlike shape for the a_3 versus a_4 plot, and a Plykin-like attractor shape in 3D. A different shape emerged for the plots involving the first three modes with CCW excitation, shown in Fig. 18(b), and there was little periodicity observed for the third and fourth mode coefficient plot.
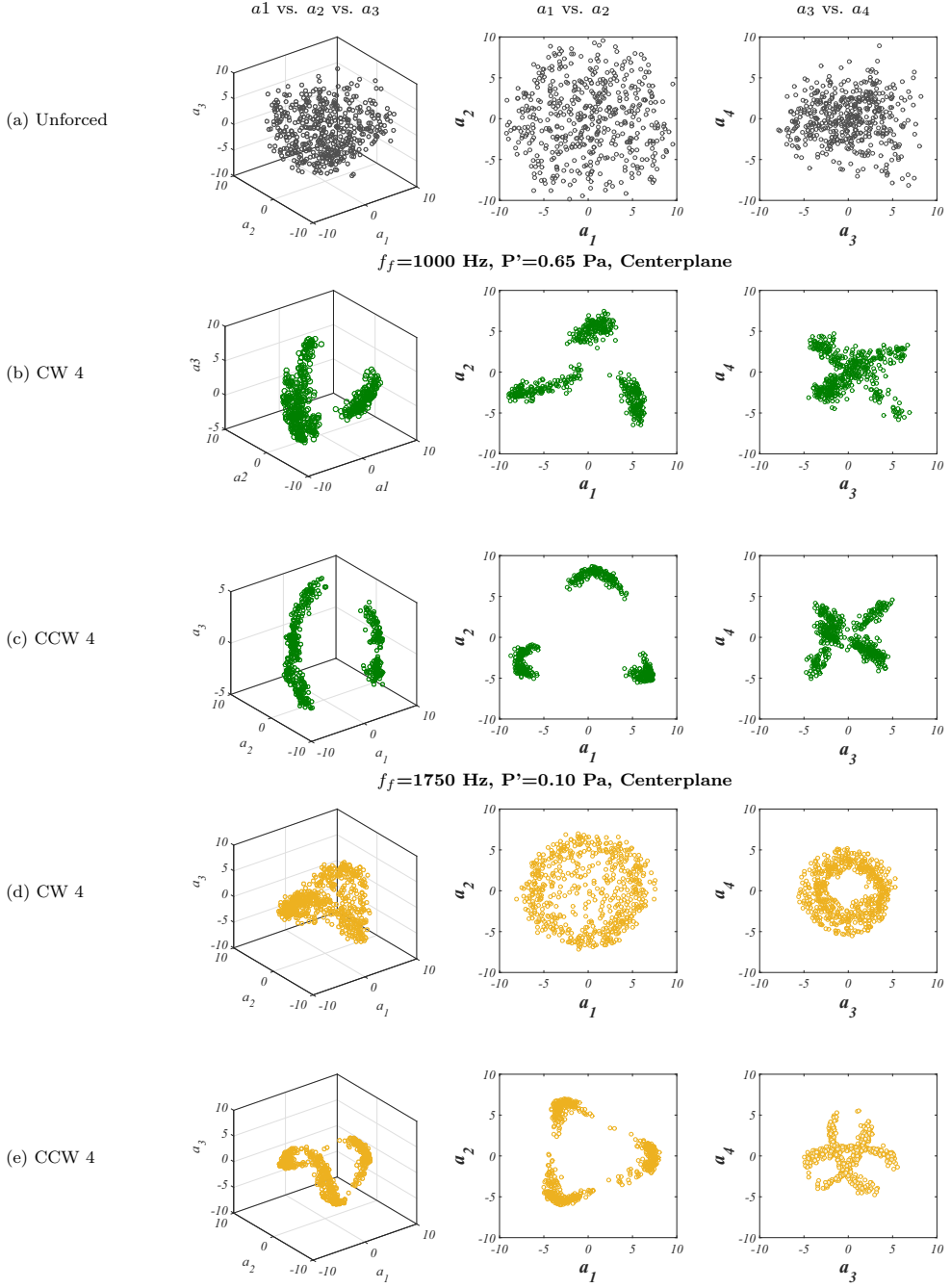
FIG. 17. PLIF POD mode coefficient plots extracted from instantaneous centerplane images of the $J = 61$ JICF: (a) Unforced; four-speaker excitation at $f_f = 1000$ Hz and 0.65 Pa for CW and CCW orientations (b), (c) and at $f_f = 1750$ Hz and 0.10 Pa for CW and CCW orientations (d), (e).
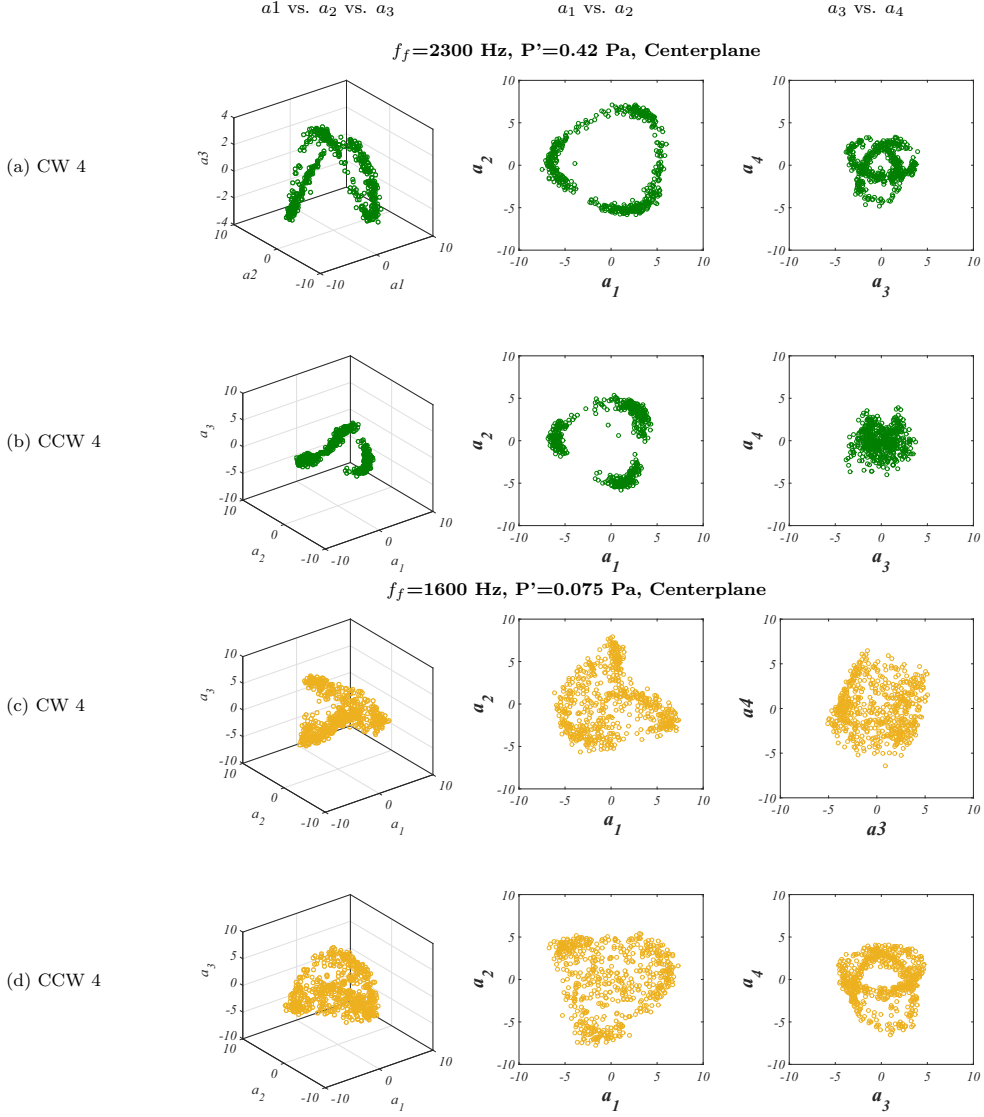
FIG. 18. PLIF POD mode coefficient plots extracted from instantaneous center-plane images of the $J = 61$ JICF: Four-speaker excitation at $f_f = 2300$ Hz and 0.42 Pa for (a) CW and (b) CCW orientations, and at $f_f = 1600$ Hz and 0.075 Pa for (c) CW and (d) CCW orientations.

Strange attractor shapes such as these have been observed in fluid flow systems subject to actuation such as pumping or forcing [60,61]. In the solution space, at most two incommensurate frequencies can appear before the appearance of the strange attractor and eventual transition to chaotic flow. For the transverse jet as well as low-density free jets, the forcing frequency f_f and fundamental frequency f_o can play the role of these incommensurate frequencies in axisymmetric excitation studies which identify quasiperiodicity as well as LI [9,21]. Poincaré maps are used to analyze the response character of the jets, representing a slice through the attractor and thereby reducing its dimension. If a system is QP, the trajectory becomes a nonrepeating orbit around a torus attractor, visualized in the Poincaré map, but if the system is chaotic, the trajectory is a nonrepeating orbit around one or more strange attractors [21,62].

In the present experiments, excitation conditions that were found or likely to produce quasiperiodicity in the USL did show a transition from the unforced bloblike shapes in phase portraits to a strange attractorlike shape, e.g., as shown in Figs. 18(c) and 18(d) for four-speaker excitation near the fundamental, $f_f = 1600$ Hz, but at an amplitude below that determined by hotwire measurements to produce LI, and hence the USL was very likely QP. These shapes contrasted the more distinctly periodic phase portraits observed for JICF excitation producing USL LI, though the difference between phase portraits for the QP USL condition and the unforced JICF [Fig. 17(a)] was still considerable.

Localized asymmetric excitation with one or two speakers in either the upstream or downstream regions produced a number of alternative strange attractorlike phase portraits, in some cases with correspondence between the shape and the previously measured (or likely) state of the USL. For example, in Fig. 19, for single speaker excitation within the fundamental frequency range, at $f_f = 1600$ Hz, and at a relatively low amplitude producing LI of the USL [Figs. 19(b) and 19(c)], there are several alternative attractor shapes, including a trefoil knot for LU, but RU and LU operation did not produce identical dynamical responses. Localized excitation in the downstream region, either on the right or left side [see Figs. 19(c) and 19(d)], also displayed characteristic attractor shapes, including the Smale-Williams as well as the trefoil and Rössler attractors, but again with differences between responses to left and right downstream excitation. The cases in Figs. 19(a)–19(d) all produced LI for the USL, per hotwire measurements. Interestingly, with localized excitation well above the fundamental regime, e.g., at a forcing frequency of 2300 Hz and a large enough amplitude to produce either USL quasiperiodicity [Fig. 19(e)] or actual LI [Fig. 19(f)], phase portraits consisted of random-appearing blobs of points, similar to the unforced JICF. These and similar examples of jet response to asymmetric excitation suggested that the state of the USL alone was not sufficient to predict the development of attractorlike phase portraits.

IV. DISCUSSION AND CONCLUSIONS

The present study utilized acetone PLIF and stereo PIV to explore the effect of localized as well as helical asymmetric excitation of the flow about a transverse jet via flush-mounted speakers oriented about the jet exit plane. Because the JICF was operated at relatively high jet-to-crossflow momentum flux ratios ($J = 61$ and 41), which in the absence of external excitation produced a naturally CU USL and asymmetric cross-sectional shape, asymmetric excitation served to alter shear layer stability as well as structural characteristics. For various excitation conditions, in many cases involving complete CW or CCW perturbations and in other cases, localized perturbations either in upstream or downstream regions, alterations in the spectral character of the USL were observed, including LI to the applied frequency and quasiperiodicity involving applied and natural frequencies. For forcing frequencies and amplitudes producing LI, in particular, asymmetric excitation was found to accelerate USL vorticity roll-up and improve mean symmetry in the jet cross section. Associated with these alterations in jet structure was the determination that molecular mixing between jet and crossflow fluid, quantified via the unmixedness parameter, was improved in both center-plane and cross-sectional slices of the jet, in particular, when USL LI was achieved. Not all excitation cases for which LI was achieved produced significant improvement in mixing, however, especially when the excitation was localized in either upstream or downstream regions about the jet exit, but also when the excitation frequency lay well above the fundamental range of USL instabilities for given jet conditions. Differences in the response of the jet's USL to forcing frequencies above or below the fundamental, e.g., as shown in the asymmetric plots in Figs. 7 and 10, were likely related to these observations of differences in mixing characteristics.

To explore further the relationship between jet dynamics and structural alterations, POD analysis was applied to the series of PLIF and PIV images, revealing distinctive 2D and 3D phase portraits or POD mode coefficient plots. In many cases, these phase diagrams revealed attractorlike topologies, especially when excitation frequencies and amplitudes produced LI of the USL, but not in all cases.
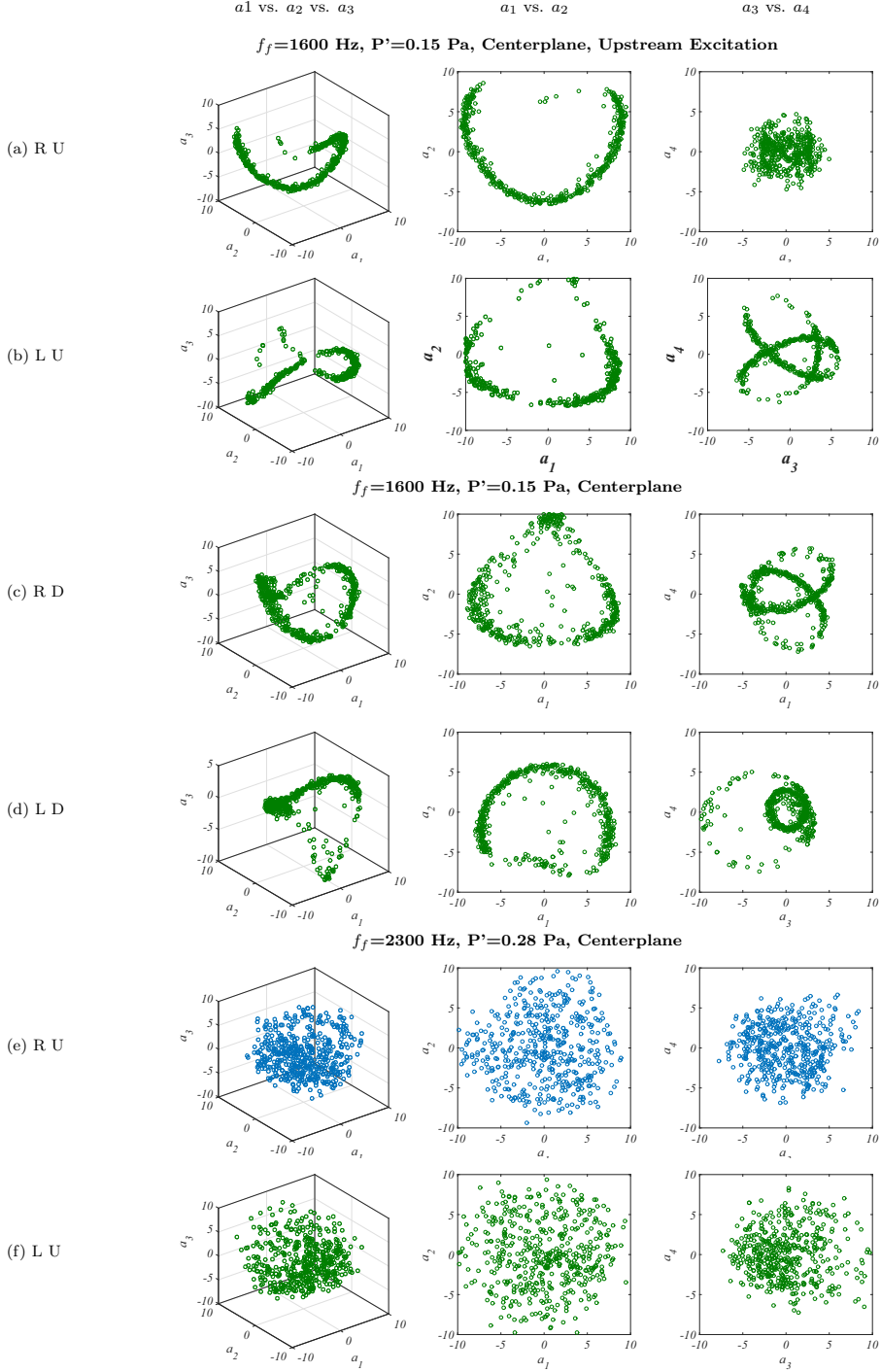
FIG. 19. PLIF POD mode coefficient plots extracted from instantaneous center-plane images of the $J = 61$ JICF: One-speaker excitation at $f_f = 1600$ Hz and 0.15 Pa for speakers positioned (a) right upstream, (b) left upstream, (c) right downstream, and (d) left downstream; and at $f_f = 2300$ Hz and 0.28 Pa for speakers positioned (e) right upstream and (f) left upstream.

In few cases did USL quasiperiodicity or LI for forcing frequencies further from the fundamental appear to create such attractor geometries.

Interestingly, in excitation cases producing POD phase portraits with strange attractor-like geometries, all corresponded to a more symmetrized jet structure, which in general produced lowered unmixedness or improved molecular mixing. This correspondence could relate to others' observations on the emergence of strange attractors in phase portraits during transitional phenomena, e.g., as observed by Guan *et al.* [63] during transition to chaos for a acoustically forced, periodic laminar flame, for cases where forcing is applied at amplitudes above the LI threshold. The transition is also characterized by the appearance of a third incommensurate frequency in the power spectral density, arising from the emergence of a second natural mode of the system. Similar features are observed in acoustically coupled laminar flame dynamics associated with single microjet burners [64], where the incommensurate frequency is associated with the transitional phenomenon of periodic flame liftoff.

In the current study, for cases in which strange attractorlike structures appeared in the POD phase space, three incommensurate frequencies were not observed in the USL power spectra. As previously discussed, in some instances the subharmonic $1/2 f_f$ and combination of the subharmonic with f_f were observed in the PSD, but these frequencies were not incommensurate with one another. Yet the existence of additional frequencies could not be ruled out in our experiments; we note that the USL spectra for the forced conditions were measured at a fixed location along the jet's USL, $s/D = 2.0$, so it is possible that additional frequencies could appear elsewhere along the jet trajectory. It is also noted that the current measurements for the USL spectra quantified the vertical component of velocity, and likely did not capture frequencies associated with $m = \pm 1$ helical modes traveling azimuthally about the jet periphery. The helical mode response is indeed important, given that in a free jet subject to axisymmetric forcing [65], in the transitional region where the helical mode is amplitude saturated, the instability can be described by a low-dimensional chaotic attractor. Hence for the transverse jet, the appearance of strange attractors may be associated with saturation of either or both of the axisymmetric and helical instability modes. Clearly, the emergence of strange attractorlike shapes in the transverse jet's PLIF- and PIV-based POD phase portraits suggested interesting transitions in the dynamical phenomena. The fact that such signatures in the phase portraits could be used as a predictor for improved mixing make the dynamics of the asymmetrically forced JICF all the more intriguing, worthy of continued exploration.

ACKNOWLEDGMENTS

[1] A. R. Karagozian, Transverse jets and their control, Prog. Energy Combust. Sci. **36**, 531 (2010).

[2] L. Gevorkyan, T. Shoji, D. R. Getsinger, O. I. Smith, and A. R. Karagozian, Transverse jet mixing characteristics, J. Fluid Mech. **790**, 237 (2016).

[3] R. M. Kelso, T. T. Lim, and A. E. Perry, An experimental study of round jets in cross-flow, J. Fluid Mech. **306**, 111 (1996).

[4] L. Cortelezzi and A. R. Karagozian, On the formation of the counter-rotating vortex pair in transverse jets, J. Fluid Mech. **446**, 347 (2001).

[5] S. Megerian, J. Davitian, L. S. de B. Alves, and A. R. Karagozian, Transverse-jet shear-layer instabilities. Part 1. Experimental studies, J. Fluid Mech. **593**, 93 (2007).

[6] R. M. Kelso and A. J. Smits, Horseshoe vortex systems resulting from the interaction between a laminar boundary layer and a transverse jet, Phys. Fluids **7**, 153 (1995).

[7] T. F. Fric and A. Roshko, Vortical structure in the wake of a transverse jet, J. Fluid Mech. **279**, 1 (1994).

[8] Z. M. Moussa, J. W. Trischka, and S. Eskinazi, The nearfield in the mixing of a round jet with a cross-stream, J. Fluid Mech. **80**, 49 (1977).

[9] T. Shoji, E. W. Harris, A. Besnard, S. G. Schein, and A. R. Karagozian, Transverse jet lock-in and quasiperiodicity, Phys. Rev. Fuids **5**, 013901 (2020).

[10] T. Shoji, A. Besnard, E. W. Harris, R. T. M'Closkey, and A. R. Karagozian, Effects of axisymetric square-wave excitation on transverse jet structure and mixing, AIAA J. **57**, 1862 (2019).

[11] T. Shoji, E. W. Harris, A. Besnard, and A. R. Karagozian, Effects of sinusoidal excitation on transverse jet dynamics, structure and mixing, AIAA J. **58**, 3889 (2020).

[12] J. Davitian, D. Getsinger, C. Hendrickson, and A. R. Karagozian, Transition to global instability in transverse-jet shear layers, J. Fluid Mech. **661**, 294 (2010).

[13] A. K. M. F. Hussain and K. B. M. Q. Zaman, The free shear layer tone phenomenon and probe interference, J. Fluid Mech. **87**, 349 (1978).

[14] T. Shoji, E. W. Harris, A. Besnard, S. G. Schein, and A. R. Karagozian, On the origins of transverse shear layer instability transition, J. Fluid Mech. **890**, A7 (2020).

[15] D. R. Getsinger, C. Hendrickson, and A. R. Karagozian, Shear layer instabilities in low-density transverse jets, Exp. Fluids **53**, 783 (2012).

[16] P. S. Iyer and K. Mahesh, A numerical study of shear layer characteristics of low-speed transverse jets, J. Fluid Mech. **790**, 275 (2016).

[17] M. A. Regan and K. Mahesh, Adjoint sensitivity and optimal perturbations of the low-speed jets in cross-flow, J. Fluid Mech. **877**, 330 (2019).

[18] E. W. Harris, A. Besnard, and A. Karagozian, Effect of tabs on transverse jet instabilities, structure, vorticity dynamics and mixing, J. Fluid Mech. **918**, A8 (2021).

[19] D. R. Getsinger, L. Gevorkyan, O. I. Smith, and A. R. Karagozian, Structural and stability characteristics of jets in crossflow, J. Fluid Mech. **760**, 342 (2014).

[20] L. Gevorkyan, T. Shoji, W. Y. Peng, and A. R. Karagozian, Influence of the velocity field on scalar transport in gaseous transverse jets, J. Fluid Mech. **834**, 173 (2018).

[21] L. K. B. Li and M. P. Juniper, Lock-in and quasiperiodicity in a forced hydrodynamically self-excited jet, J. Fluid Mech. **726**, 624 (2013).

[22] K. Kashinath, L. K. B. Li, and M. P. Juniper, Forced synchronization of periodic and aperiodic thermoacoustic oscillations: lock-in, bifurcations and open-loop control, J. Fluid Mech. **838**, 690 (2018).

[23] J. Davitian, C. Hendrickson, D. Getsinger, R. T. M'Closkey, and A. R. Karagozian, Strategic control of transverse jet shear layer instabilities, AIAA J. **48**, 2145 (2010).

[24] E. W. Harris, T. Shoji, A. Besnard, S. G. Schein, R. T. M'Closkey, L. Cortelezzi, and A. R. Karagozian, Effects of controlled vortex generation and interactions in transverse jets, Phys. Rev. Fluids **7**, 013902 (2022).

[25] P. V. Danckwerts, The definition and measurement of some characteristics of mixtures, Appl. Sci. Res. **3**, 279 (1952).

[26] S. H. Smith, The Scalar Concentration Field of the Axisymmetric Jet in Crossflow, Ph.D. thesis, Stanford University, Department of Mechanical Engineering, 1996.

[27] A. Kukukova, J. Aubin, and S. M. Kresta, A new definition of mixing and segregation: Three dimensions of a key process variable, Chem. Eng. Res. Des. **87**, 633 (2009).

[28] J. E. Broadwell and R. E. Breidenthal, Structure and mixing of a transverse jet in incompressible flow, J. Fluid Mech. **148**, 405 (1984).

[29] L. K. B. Li and M. P. Juniper, Lock-in and quasiperiodicity in hydrodynamically self-excited flames: Experiments and modeling, Proc. Combust. Inst. **34**, 947 (2013).

[30] G. Batchelor and A. Gill, Analysis of the stability of axisymmetric jets, J. Fluid Mech. **14**, 529 (1962).

[31] A. Michalke, Survey on jet instability theory, Prog. Aerosp. Sci. **21**, 159 (1984).

[32] G. E. Mattingly and C. C. Chang, Unstable waves on an axisymmetric jet column, J. Fluid Mech. **65**, 541 (1974).

[33] P. Plaschko, Helical instabilities of slowly divergent jets, J. Fluid Mech. **92**, 209 (1979).

[34] S. Leibovich, Vortex stability and breakdown: Survey and extension, AIAA J. **22**, 1192 (1984).

[35] P. J. R. Strange and D. G. Crighton, Spinning modes on axisymmetric jets. part 1, J. Fluid Mech. **134**, 231 (1983).

[36] F. Gallaire and J. M. Chomaz, Mode selection in swirling jet experiments: A linear stability analysis, J. Fluid Mech. **494**, 223 (2004).

[37] S. C. Crow and F. H. Champagne, Orderly structure in jet turbulence, J. Fluid Mech. **48**, 547 (1971).

[38] J. Cohen and I. Wygnanski, The evolution of instabilities in the axisymmetric jet. Part 1. The linear growth of disturbances near the nozzle, J. Fluid Mech. **176**, 191 (1987).

[39] S. M. Kusek, T. C. Corke, and P. Reisenthel, Seeding of helical modes in the initial region of an axisymmetric jet, Exp. Fluids **10**, 116 (1990).

[40] T. C. Corke and S. M. Kusek, Resonance in axisymmetric jets with controlled helical-mode input, J. Fluid Mech. **249**, 307 (1993).

[41] I. Gursul, Effect of nonaxisymmetric forcing on a swirling jet with vortex breakdown, J. Fluids Eng. **118**, 316 (1996).

[42] L. S. d. B. Alves, R. E. Kelly, and A. R. Karagozian, Local stability analysis of an inviscid transverse jet, J. Fluid Mech. **581**, 401 (2007).

[43] L. S. d. B. Alves, R. E. Kelly, and A. R. Karagozian, Transverse-jet shear-layer instabilities. part 2. linear analysis for large jet-to-crossflow velocity ratio, J. Fluid Mech. **602**, 383 (2008).

[44] L. Gevorkyan, Structure and Mixing Characterization of Variable Density Transverse Jet Flows, Ph.D. thesis, University of California, Los Angeles, 2015.

[45] A. Lozano, Laser-Excited Luminescent Tracers for Planar Concentration Measurements in Gaseous Jets, Ph.D. thesis, Stanford University, Department of Mechanical Engineering, 1992.

[46] T. Shoji, Mixing and Structural Characteristics of Unforced and Forced Jets in Crossflow, Ph.D. thesis, University of California, Los Angeles, 2017.

[47] D. R. Getsinger, Shear Layer Instabilities and Mixing in Variable Density Transverse Jet Flows, Ph.D. thesis, University of California, Los Angeles, 2012.

[48] L. K. Su and M. G. Mungal, Simultaneous measurements of scalar and velocity field evolution in turbulent crossflowing jets, J. Fluid Mech. **513**, 1 (1999).

[49] K. Canzonieri, Experimental Studies on Low Density Jets in Crossflow, master's thesis, University of California, Los Angeles, Department of Mechanical and Aerospace Engineering, 2009.

[50] A. C. Besnard, External Asymmetric Forcing of Convectively Unstable Transverse Jets, Ph.D. thesis, University of California, Los Angeles, Department of Mechanical and Aerospace Engineering, 2019.

[51] K. R. Sreenivasan, S. Raghu, and D. Kyle, Absolute instability in variable density round jets, Exp. Fluids **7**, 309 (1989).

[52] P. Huerre and P. A. Monkewitz, Local and global instabilities in spatially developing flows, Annu. Rev. Fluid Mech. **22**, 473 (1990).

[53] M. P. Juniper, L. K. B. Li, and J. W. Nichols, Forcing of self-excited round jet diffusion flames, Proc. Combust. Inst. **32**, 1191 (2009).

[54] L. Sirovich, Turbulence and the dynamics of coherent structures, Quart. Appl. Math. **45**, 561 (1987).

[55] K. E. Meyer, J. M. Pedersen, and O. Özcan, A turbulent jet in crossflow analysed with proper orthogonal decomposition, J. Fluid Mech. **583**, 199 (2007).

[56] P. Schlatter, S. Bagheri, and D. S. Henningson, Self-sustained global oscillations in a jet in crossflow, Theor. Comput. Fluid Dyn. **25**, 129 (2011).

[57] R. Vernet, L. Thomas, and L. David, Analysis and reconstruction of a pulsed jet in crossflow by multiplane snapshot POD, Exp. Fluids **47**, 707 (2009).

[58] H. Poincaré, Mémoire sur les courbes définies par une équation différentielle (I), J. Mathémat. Pures Appliq. **7**, 375 (1881).

[59] G. Bidan, C. Vezier, and D. Nikitopoulos, Study of unforced and modulated film-cooling jets using proper orthogonal decomposition, Part 2: Forced jets, J. Turbomach. **135**, 021038 (2013).

[60] G. Berkooz, P. Holmes, and J. L. Lumley, The proper orthogonal decomposition in the analysis of turbulent flows, Annu. Rev. Fluid Mech. **25**, 539 (1993).

[61] J. Miles, Strange attractors in fluid dynamics, Adv. Appl. Mech. **24**, 189 (1984).

[62] S. H. Strogatz, in *Nonlinear Dynamics and Chaos with Applications to Physics, Biology, Chemistry, and Engineering* (Perseus Books, Reading, MA, 1994), pp. 317–335.

[63] Y. Guan, M. Murugesan, and L. K. B. Li, Strange nonchaotic and chaotic attractors in a self-excited thermoacoustic oscillator subjected to external periodic forcing, Chaos **28**, 093109 (2018).

[64] H. S. Sim, A. Vargas, D. D. Ahn, and A. R. Karagozian, Laminar microjet diffusion flame response to transverse acoustic excitation, Combust. Sci. Technol. **192**, 1292 (2020).

[65] M. Bonetti and J.-P. Boon, Chaotic dynamics in open flow: The excited jet, Phys. Rev. A **40**, 3322 (1989).